3-21-2017

Fatty Acid Biomarker Detection for Breast Cancer Using Differential Mobility Spectrometry with Non-Radioactive Ion Source

James Joseph Alberti
University of South Florida, jjalbert@mail.usf.edu

Fatty Acid Biomarker Detection for Breast Cancer Using Differential Mobility Spectrometry with Non-Radioactive Ion Source

by

James J. Alberti

A thesis submitted in partial fulfillment
of the requirements for the degree of
Master of Science in Electrical Engineering
Department of Electrical Engineering
College of Engineering
University of South Florida

Major Professor: Andrew Hoff, Ph.D.
Stephen E. Saddow, Ph.D.
Richard Gilbert, Ph.D.

Date of Approval:
March 13, 2017

Keywords: Ion Mobility Spectrometry, Mass Spectrometry, Planar Sensor, Coaxial Sensor, High-Field Asymmetric-Waveform

DEDICATION

Thank you to my loving parents who have sacrificed their time, effort and personal finances to provide me the opportunity to receive a quality education that has given me the foundation for attaining an advanced degree in later years.

To my wife whose love and support have given me peace and warmth of heart that has allowed me to stay focused and motivated on achieving my educational goals.

To God who has given me the gifts and opportunities to develop my skills so that I may apply them towards the benefit of mankind. Thank you.

ACKNOWLEDGMENTS

I am grateful for the guidance and assistance that Dr. Andrew Hoff, my graduate advisor and major professor, provided throughout my graduate studies. I also thank him for his feedback during my thesis research and his help in editing this document. Thank you to Dr. Stephen E. Saddow for his guidance on thesis format and preparation and for agreeing to be part of my committee. He always made himself available to answer any questions I had about the process. Thank you to Dr. Richard Gilbert for his willingness to give of his time to be part of my committee. I am also grateful to Spiros Manolakos, an Analytical Chemist and former colleague, who assisted with the initial DMS instrument setup for this work and his guidance on testing, sampling technique, and application software instruction.

Without the help of Dr. Erkinjon Nazarov, this work would not be possible. He introduced me to DMS technology during the four years we worked together at Draper Laboratory and it is his knowledge and expertise in the field, along with his willingness to instruct, that inspired me to propose using DMS as the core technology of this work. Dr. Nazarov provided the DMS instrument used in this research, supplied literature on the technology, answered countless questions on theory and operation of DMS, and provided guidance throughout my work. I am grateful for the knowledge he has shared with me, the opportunity to have worked alongside him, and for his friendship.

TABLE OF CONTENTS

LIST OF TABLES

LIST OF FIGURES

ABSTRACT

Differential Mobility Spectrometry (DMS) using a non-radioactive ion source (NRIS) is investigated as a possible medical diagnostic instrument for near real-time detection of breast cancer biomarkers. In previous clinical studies, concentrations of Linoleic, Palmitic and Stearic fatty acids have been observed at different levels in women with carcinoma breast cancer versus women with benign tumors or healthy women showing no signs of breast cancer. Present diagnostic methods require a biopsy of the suspect tissue and a microscopic lab analysis performed to determine its disease state. This process can take hours or days before the patient and doctor are informed of the results. Controlled volumetric samples of each fatty acid listed above were introduced into a DMS instrument, using a NRIS, to determine detectability of each acid. The results provide proof-of-concept that Linoleic, Palmitic and Stearic fatty acids can be uniquely identified by varying the sample temperature and scanning the ionized fatty acid molecules in both the negative and positive ion mode of the DMS instrument. Detection response times range from 2 to 6 seconds for initial detection up to 35 seconds for peak detection. The Limit of Detection for the DMS instrument is estimated in the low parts per billion.

CHAPTER 1: INTRODUCTION

Breast cancer is the second leading cause of cancer death in women, second only to lung cancer. In 2017, 40,610 women are expected to die from the disease [1]. Early detection of breast cancer is critical to maximizing a patient's ability for disease recovery and minimizing the loss of breast tissue. Existing diagnostic methods include Mammograms, X-ray, Ultrasound, and Magnetic Resonance Imaging. When a cyst is discovered, a small sample of suspect tissue must be removed via biopsy or surgery for analysis by a pathologist under microscope, which can take several days to a week or more, during which most patient's experience strong emotions of anxiety, fear, anger, and sadness while waiting for test results [2]. Developing a real-time diagnostic instrument that provides immediate disease state indication of biopsied tissue can alleviate the patient from unnecessary concern when the analyzed results indicate benign tissue and provide the opportunity for immediate surgical removal of cancerous tissue. During surgery, a real-time diagnostic instrument may provide the physician with immediate feedback as tissue is removed, helping to ensure elimination of all cancerous tissue and minimizing the margins of lost good tissue. This reduces the risk of subsequent operations needed to remove cancerous tissue if not completely removed in the initial surgical procedure. In recent years, research has been conducted using mass spectrometry to classify brain tumors and maximize tumor resection while preserving brain function [3] [4] [5]. However, mass spectrometers typically require introduction of pure samples to provide good mass spectra [6]. Existing technology to purify samples before introduction into a mass spectrometer include Gas Chromatography (described in section 2.1) and

Liquid Chromatography, which can take 2 to 30 minutes or more for target gas separation, depending on the chemical, system temperature, and desired resolution [7].

A promising instrument recently developed by Dr. Zoltan Takats, working at Imperial College London, is the iKnife (Rapid Evaporative Ionization Mass Spectrometer). The iKnife vaporizes and converts tissue into gas-phase ionic species, via bipolar forceps, that aspirate into a mass spectrometer. The lipid profiles of the tissue are analyzed and within seconds, a diagnosis is rendered on the histological state of the sample. In a recent study published in the journal Science Translational Medicine, July 2013, the iKnife ex vivo oncological analysis of cancerous and noncancerous tissue (stomach, colon, cecum, liver, lung, breast, and brain) matched the postoperative histological diagnosis in 100% (81 samples) of the cases studied. Intraoperative in vivo results of the iKnife, sampling similar tissue, matched 96.5% with post histological diagnosis, 3.5% indicating both false-positive and false negative results [8]. However, the approximate cost of iKnife is $380,000 US, which may be prohibitive for many hospitals and surgical centers [9].

Differential Mobility Spectrometry (also known as FAIMS – High-field asymmetric-waveform ion mobility spectrometry) is a technology that may provide immediate feedback to the user (within seconds) by sampling gas molecules, ionizing then filtering the ions for detection. DMS separates and identifies ionized gas molecules at atmospheric pressure, based on their mobility in a high voltage asymmetric RF waveform coupled with a static DC or low frequency waveform. Coupling a DC or low frequency waveform to the RF waveform allows DMS to be used as a scanning electronic gas molecule filter, allowing only targeted ionized molecules to pass through its electrodes to an ion sensor for detection in near real-time [10]. It can also act as a prefilter to a mass spectrometer, providing gas samples of desired ions.

DMS is currently being used in non-medical applications, such as air quality monitoring on the International Space Station, using a Draper Laboratory developed instrument called the microAnalyzer [11]. DMS is also being used for chemical trace and explosives detection by the military with the JUNO instrument, which was developed by Chemring Sensors & Electronic Systems in collaboration with Draper Laboratory [12]. Research is being conducted using DMS in nuclear forensics for rapid separation of samples for inorganic analyses before being analyzed in a field deployable mass spectrometer [13].

Widespread use of DMS in medical applications has been limited because of the low-grade radioactive ion source (Ni-63) used in the device to ionize the incoming gas sample for analysis, which necessitates government licensing and tracking [14]. However, a scientific team at Draper Laboratory comprising of Dr. Erkinjon Nazarov (Senior Scientist), Spiros Manolakos (Analytical Chemist), Dr. Timothy Postlethwaite (Program Manager), and Jim Alberti (Senior Member Technical Staff – Electrical), recently developed a non-radioactive ion source (NRIS) which replaces Ni-63 and eliminates the need for government licensing and tracking, opening up the technology for use in medical applications. Draper Laboratory filed a patent application for the NRIS with the USPTO on February 3, 2016, U.S. Application Number: 15/014,771. The estimated cost of the DMS instrument using a NRIS, such as in this work, is approximately $10,000 US.[1]

Investigations are now underway to determine how DMS can be applied to biomedical applications in detecting various disease states. A recent clinical study conducted by Brigham Women's Hospital in collaboration with Draper Laboratory used DMS, in combination with Gas Chromatography (GC), to analyze the breath of patients suspected of having invasive aspergillosis, a fungal pneumonia with nonspecific symptoms. Traditional testing for this disease sometimes

[1] The author has designed analytical systems with the same DMS model used in this work and has detailed knowledge of the instrument component design and cost.

requires a lung biopsy and is slow to yield results (days or weeks). Using a DMS based system allows clinicians to non-invasively detect the disease within minutes, well in advance of existing methods [15]. Early detection allows clinicians to begin treatment sooner so that recovery rates are maximized and mortality rates minimized.

1.1. Thesis Objective

This thesis will investigate the feasibility of using DMS technology with a non-radioactive ion source to detect Linoleic, Palmitic, and Stearic fatty acids, which in previous clinical studies were identified as potential biomarkers for breast cancer screening using a GC-Mass Spectrometer instrument [16] [17] [18]. A controlled gas sample volume of each fatty acid at various temperatures will be introduced into the DMS to determine if the acids are detectable by the instrument and the approximate time required for detection. Results will be compared for differentiation between the fatty acids and determine if they can be uniquely identified. The headspace saturation concentration for each fatty acid sampled will be calculated at 25°C and an estimate made of the Limit of Detection for the DMS instrument.

1.2. Thesis Outline

Chapter 2 describes the theory and operation of both the DMS instrument and non-radioactive ion source. Chapter 3 states the test setup and methods used for testing. Chapter 4 reports the experimental results for each fatty acid sample. Chapter 5 summarizes the test results and describes any observed issues or possible sources of error in the results. The chapter concludes with describing the viability of using DMS for breast cancer biomarker detection and discusses areas for future work.

CHAPTER 2: THEORY

2.1. History

One of the earliest methods of separating gas molecules, paper chromatography, was developed in 1903 by Russian scientist Mikhail Semenovich Tswett to separate plant pigments. From this, gas chromatography developed and in the 1950's its methods were refined to what is now considered modern day gas chromatography. GC techniques are widely used in analytical chemistry and rely on a molecules' physical and chemical properties to separate itself from other chemical species as the sample gas travels through a narrow tube or column (typically glass or metal) coated with a microscopic layer of polymer on the inner walls of the tube. As the sample gas travels down the column and interacts with the polymer coating, adsorption inhibits the constituent components of the gas causing each chemical component to travel along the column at different rates, which provides chemical separation. A detector senses each component as it emerges from the column, identifying the type and amount of each chemical. Detection times vary based on length and construction of the tube, polymer coating, and the adsorption strength of the sample gas [19] . Times may vary from several minutes to 30 minutes or more for better separation.

Gas separation may be achieved electrically using Ion Mobility Spectrometry (IMS), a precursor to DMS, which was developed in the 1950's and 1960's by Earl W. McDaniel of Georgia Institute of Technology. It separates and identifies gas molecules based on time-of-flight (TOF) through a drift tube with an applied electric field in a drift gas (typically air or N_2) at ambient pressure. The ionized analyte gas, which contains ions of several species, is introduced into the

drift tube where it is subjected to an electric field for ion direction and an opposing buffer gas. The molecules of the buffer gas collide with the analyte molecules and segregate based on their properties of mass, charge, size and shape. The larger the collision cross-section of the analyte molecule (i.e. an ion's surface area available for collision), the greater the probability for buffer gas collisions to occur and impede the analytes' molecular travel along the tube. A sensor at the opposite end of the tube detects the various ion species as they exit, each having a unique TOF through the tube based on physical and electrical properties (Figure 1) [10] [20].

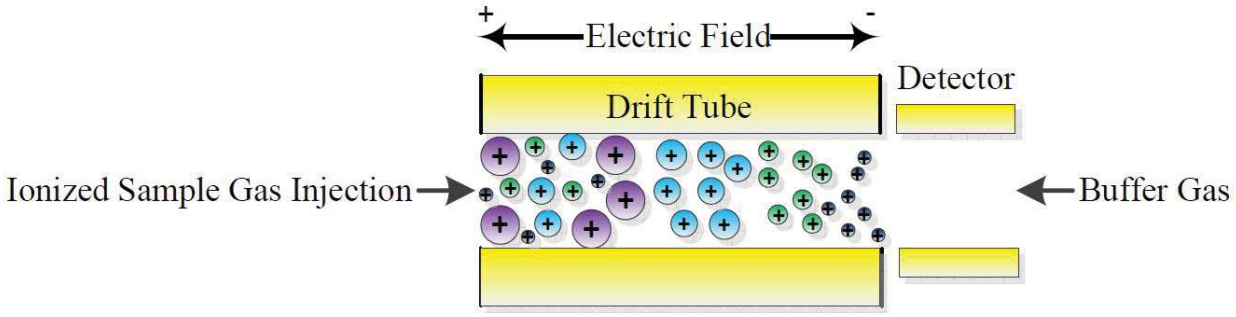

Figure 1 Ion Mobility Spectrometer Drift Tube

Equation (1) shows the IMS velocity of individual ions when subjected to an electric field,

$$V_i(t) = K_i(t) * E(t) \quad (1)$$

where V_i (cm/s) is the ion velocity for individual ion species, K_i (cm^2/v-sec) is the ion mobility of the particular ion and E (v/cm) is the magnitude of the electric field, relative to time (t) [10].

Because IMS detection is based on time-of-flight principles, the ionized gas sample must be pulsed into the drift tube, which has a minimum period of V_i (t), being limited by ions with the lowest coefficient of mobility (K_i). Also, ions that have a similar coefficient of mobility cannot be separated and uniquely identified from each other, placing limits on gas detection.

2.2. Differential Mobility Spectrometry Development

DMS utilizes differences in an ion's high field mobility from its low field mobility properties to provide ion filtering. The technology was originally proposed in the Soviet Union during the 1980's by M. Gorshkov and later developed by Igor Buryakov and his colleagues, who implemented the first practical DMS instrument, which was described to Western scientists in the article, "Separation of ions according to their mobility in a strong alternating current electric field," by I.A. Buryakov, E.V. Krylov, A.L.Makas, E.G. Nazarov, V.V. Pervukhin, and U.Kh. Rasulev, Sov.Tech.Phys. Lett. 17(6), 1991, p 446" [21]. This work found that an ion's trajectory through an electric field is non-linear when exposed to a perpendicularly applied high electric field (E > 1000 V/cm) vs a low electric field. Also, ions having similar low field trajectories can have significantly different high field trajectory, allowing detection between the two. This distinction is what allows filtering of different ion species and is the basis of DMS [10] [22].

In the late 1980's and early 1990's, two major thrusts developed in the sensor design exposing ions to the asymmetric high RF electric field: one using parallel planar electrodes and the other using coaxial (cylindrically curved) electrodes. Table 1 lists the primary characteristic differences between the two types of electrode designs [23].

Table 1 Characteristic Comparison of Coaxial and Planar Sensor Electrode Design

CHARACTERISTICS	COAXIAL SENSOR	PLANAR
Response Time Example: M+(H2O)n and (H3O)+(H2O)n ions	Two orders of magnitude slower. 200ms	Faster 2.5ms
Concentration of Detected Ions	Higher (when focus conditions met)	Lower
High Field Mobility Detection	Ions with weaker HF mobility not detectable	Ions with weaker HF mobility detectable
Simultaneous Detection Capability of Positive and Negative Ions	No	Yes

Because the parallel planar electrode sensor offers faster response time and increased detectability of ions with less dependence on high field mobility sensitivity, this work will focus on the theory and test results using a parallel planar electrode design.

2.3. Differential Mobility Spectrometer Architecture and Operation

Figure 2 shows the architecture of a DMS instrument used to target specific gas ions. The figure displays how positively charged plasma ions traveling through the system combine with the neutral gas sample to form positively charged analyte which is directed to the planar electrodes for filtering and detection. Likewise, by reversing the NRIS electric field direction, electrons are directed towards and attach to the neutral gas sample to form negatively charged analyte for filtering and detection. Adjusting the Transport Gas flow rate (0 to 750 sccm purified air), Counterflow rate (0 to 300 sccm purified air), NRIS electric field magnitude (0 to 260 V/cm),

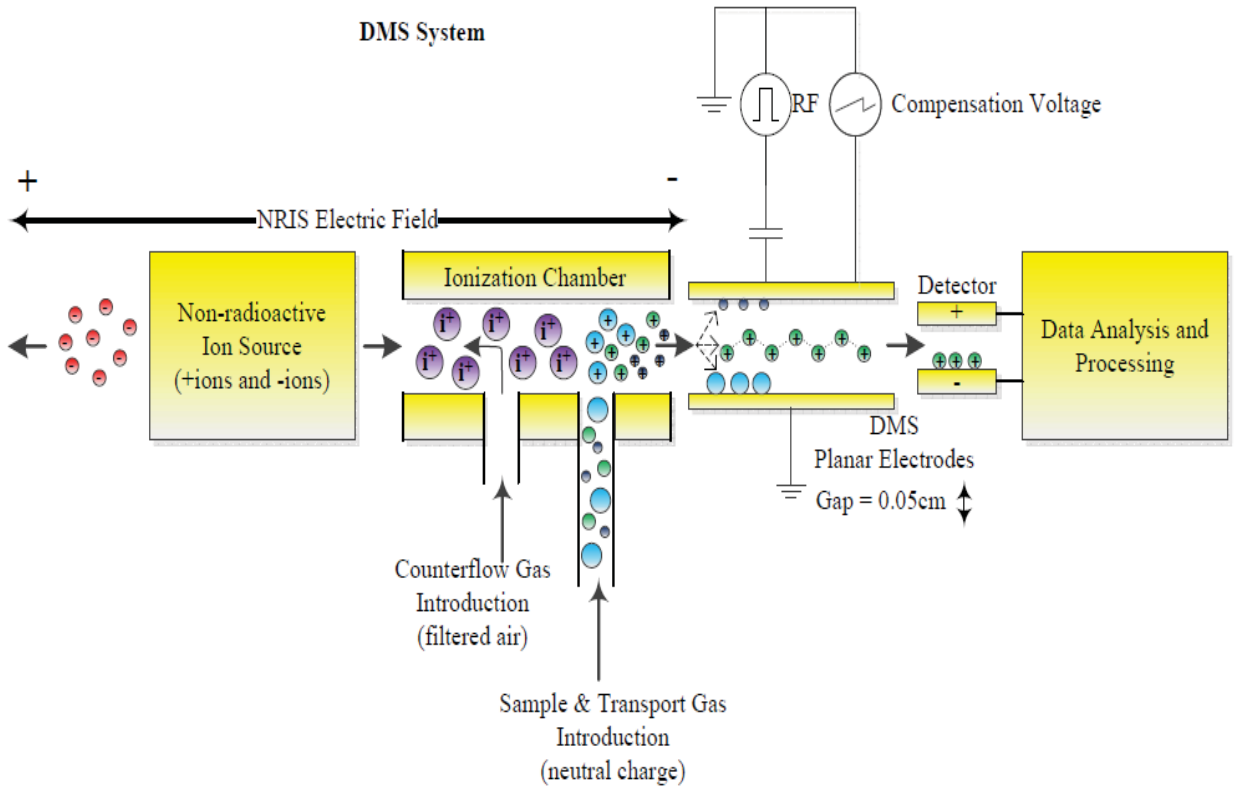

Figure 2 DMS System Architecture Showing Selection of a Specific Positive Ion

electric field direction, the RF amplitude (+500V to +1350V peak) and the Compensation voltage amplitude (-30V to +10V) using the waveforms shown in Figure 3, different gas ions are selected and allowed to pass through the DMS electrodes to the ion detector. For a planar electrode gap = 0.05cm, the RF high-field = 10kV/cm for V_1 = +500V, 27kV/cm for V_1 = +1350V.

When the gas sample is introduced into the DMS system, its neutrally charged molecules (which may be a mixture of various molecules in addition to the target molecules) enter the ionization chamber, where they interact with ions of various charge from the NRIS. The interaction of the NRIS ions with the sample gas molecules causes electrons to be either removed or added to the sample gas molecules, forming positively or negatively charged analyte, respectively. The NRIS electric field direction is selected to move the desired ion polarity towards the planar electrodes and detector and oppositely charged (unwanted) ions away from the electrodes. The NRIS electric field direction chosen depends on whether the target gas has an affinity for donating or accepting an electron, which determines if it will have a positive or negative charge, when collisions occur with the NRIS ions. The transport gas is used to assist in directing the sample gas towards the ionization chamber. The counterflow gas helps in removing unwanted ions and the plasma by-product, nitrogen oxide (NO_x), away from the ionization chamber. When gas sample ions enter the planar electrodes, they are exposed to high and low electric fields, perpendicular to the planar electrodes, which are generated by the RF waveform (discussed in detail below). The nonlinear response of the ion to the high and low perpendicular electric field causes a slow drift towards one or the other electrode. Ion species having the same low-field response may have substantially different high field response [22].

When the RF and Compensation voltages are turned off, the NRIS electric field and transport gas directs all ions of a particular polarity axially through the planar electrodes to the detector with no filtering of individual ions.

When the RF voltage is turned on, ions entering the planar electrodes are subjected to an alternating high-field and low-field periodic asymmetric waveform, perpendicular to the electrode surface, at an approximate frequency = 1.2MHz with a duty cycle = 30%. Referencing Figure 3, the maximum amplitude V_1 is user adjustable within a range of +500V to +1350V and voltage V_2 automatically adjusts such that a 0V DC offset is maintained. The short pulse of the RF waveform exposes the ion to a high-field force driving it radially towards one electrode followed by a longer low-field pulse of opposite polarity, which exerts the same net force in the opposite direction, driving the ion towards the other electrode. The voltage and time product for both the high-field and low-field portions of the waveform are equal but opposite, resulting in a net zero DC drift force exerted to the ion by the RF waveform. The high electric field (E > 1000V/cm) exerted by the RF waveform followed by the low electric field, causes the ion to experience physical changes that cause the ion to have a non-linear trajectory through the DMS electrodes. This non-linear trajectory results in a DC bias shift towards one electrode or the other, represented by an α (alpha) parameter (Equation 3), resulting in fast oscillation and slow drift of the ion to the electrodes (Figure 4). Some of the physical changes that occur to cause the DC shift are clustering, declustering and fragmentation of ions, changes in the cross-sectional area, and elongation of the ion structure. Without an additional DC compensation voltage to offset the ions' DC bias shift, the ions are neutralized on either electrode. However, if a DC compensation voltage is added to the RF waveform, then, at a specific compensation voltage value, the ions' DC bias shift is counter-balanced by the added DC voltage such that the bias towards either electrode in both high-field

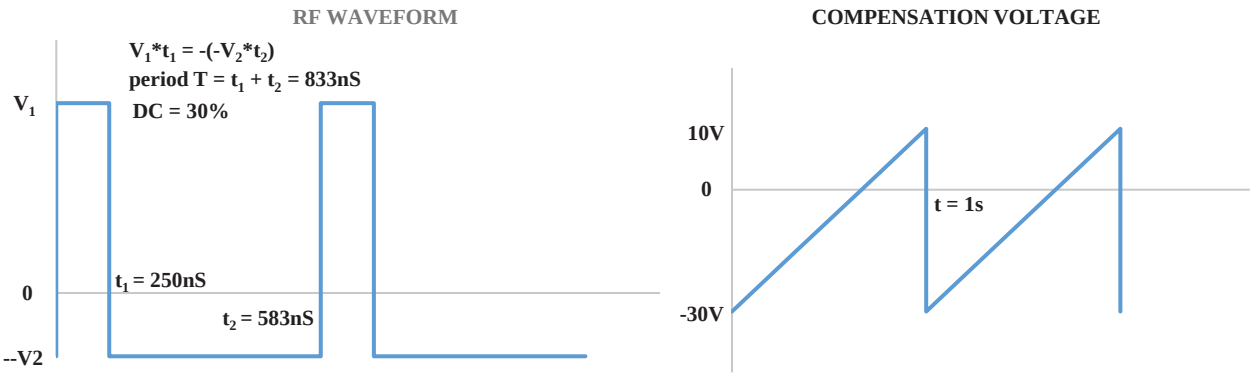

Figure 3 RF Asymmetric and Compensation Voltage Waveforms

and low-field conditions is removed and the ion is allowed to travel axially through the planar electrodes to the ion sensor for detection. All other ion species are neutralized on either of the two planar electrodes (due to differences in their α parameter) and prevented from reaching the detector (Figure 4). The resulting spectra is a plot showing the amount of detected charge (intensity) at the specific DC compensation voltage (see Chapter 4: Experimental Results).

Scanning for multiple ion species can be achieved by varying the compensation voltage rather than using a static DC voltage. The right graph of Figure 3 shows a low frequency sawtooth waveform, which has a typical frequency of 1Hz and varies in voltage amplitude from -30V to +10V. The resulting spectra is a plot showing the amount of detected charge for each ion species relative to the compensation voltage where each species is detected.

The mobility of an ion in a DMS system can be written as shown in Equation (2),

$$K\left(\frac{E}{N}\right) = K(0)[1 + \alpha\left(\frac{\mathrm{E}}{\mathrm{N}}\right)] \quad (2)$$

where K is the ion mobility, E is the electric field magnitude, N is the gas number density calculated from the ideal gas law, (E/N) expressed in Townsends (Td) describes electric field magnitude as well as gas collisions, K(0) is the ion mobility coefficient under low-field conditions and α (E/N) (unitless number << 1) is the normalized alpha function, a unitless value, representing

the ions' trajectory change when exposed to a high versus a low electric field [22]. Equation (2) can be rewritten to express the alpha function as shown in Equation (3),

$$\alpha\left(\frac{E}{N}\right) = \frac{K\left(\frac{E}{N}\right) - K(0)}{K(0)} = \frac{\Delta K\left(\frac{E}{N}\right)}{K(0)} \tag{3}$$

where $\Delta K\left(\frac{E}{N}\right)$ is the difference in high field to low field mobility and $\alpha\left(\frac{E}{N}\right)$ expresses the ratio of the differential mobility relative to the low field ion mobility K(0).

If the electric field relative to gas density is very low (E/N small) then $\alpha\ (E/N)$ = 0 and $K(E/N)$ = K(0). Alternatively, if the electric field relative to gas density is high (E/N large) then α is the normalized difference between the high field and low field mobility response. Figure 4 shows the ion trajectory based on its high field versus low field response for the following alpha function conditions:

1. high field mobility greater than low field mobility (α > 0)
2. high field mobility equal to low field mobility (α = 0)
3. high field mobility less than low field mobility (α < 0)

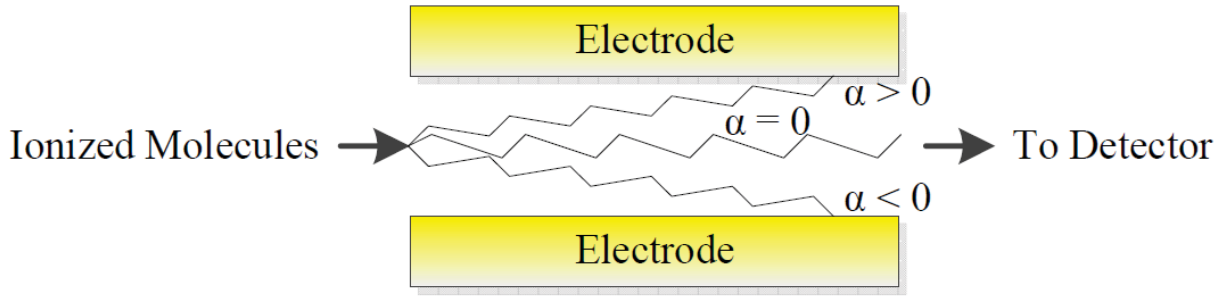

Figure 4 Ion Trajectory as a Function of Alpha Value

2.4. Non-Radioactive Ion Source Architecture and Operation

The Non-Radioactive Ion Source provides the necessary positive and negative charges used to ionize gas samples. Previous ion generators utilized radioactive material, such as Ni-63, limiting use of the DMS instrument to applications willing to abide by the United States Nuclear Regulatory

Committee 10 CFR Part 31 requirements for licensing and tracking of radioactive material [14]. With the development of a non-radioactive ion source, government regulation and tracking is no longer an issue and DMS technology can now be applied to generalized applications, including medical.

Figure 5 shows the architecture of the NRIS, which is designed to operate under direct computer control (using a serial communications port) or stand-alone via pre-programmed parameters. The frequency and duty cycle of the plasma generator are controlled to allow adjustability of the quantity of generated ions and to limit the undesirable by-product, NO_x, which forms when plasma is generated in air at atmospheric pressure (similar to lightening). During my work on the Draper team for the NRIS, we learned that the drawback of generating NO_x (which is not present in Ni-63) is that it absorbs the free electrons generated from plasma, making them unavailable for ionizing the sample gas molecules and lowering the probability of target gas detection. However, by raising the frequency and lowering the duty cycle of the plasma source, the time that the plasma is activated is minimized, which minimizes the amount of NO_x produced and leaves sufficient ions available for ionization.

A high DC offset voltage is added to the oscillator circuit to establish a NRIS electric field that directs positively or negatively formed ions (selected by the ion polarity switch setting) towards the ionization chamber for gas molecule ionization (Figure 2). The plasma detection sensor provides closed loop feedback to the microcontroller for automatic adjustment of the plasma generator to maintain consistent ion generation over the life of the instrument. The NRIS and DMS architectures described in this chapter form the design of the instrument used for this work.

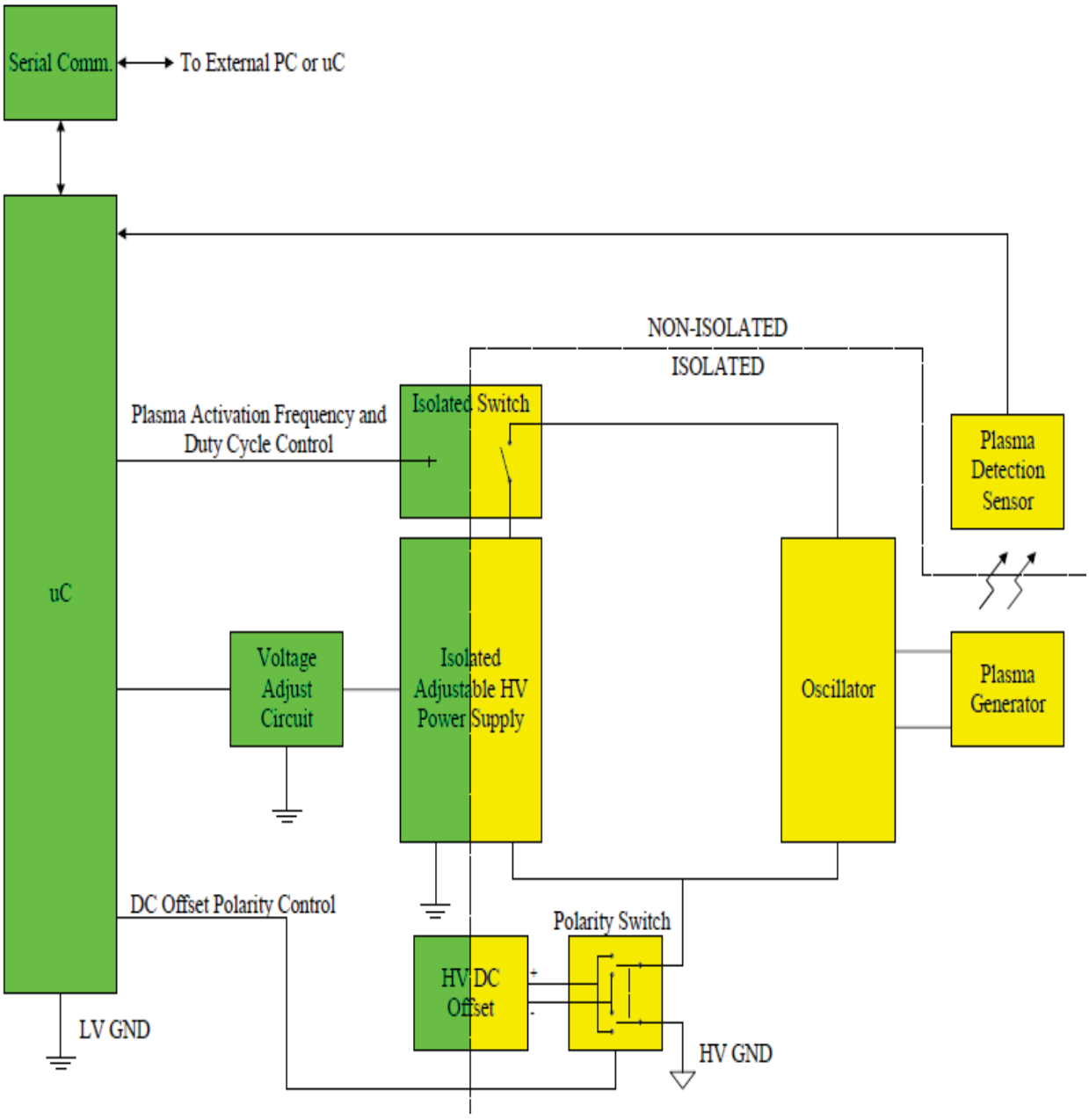

Figure 5 NRIS Architecture Design

CHAPTER 3: TEST SETUP AND METHOD

3.1. Differential Mobility Spectrometer Test System and Setup

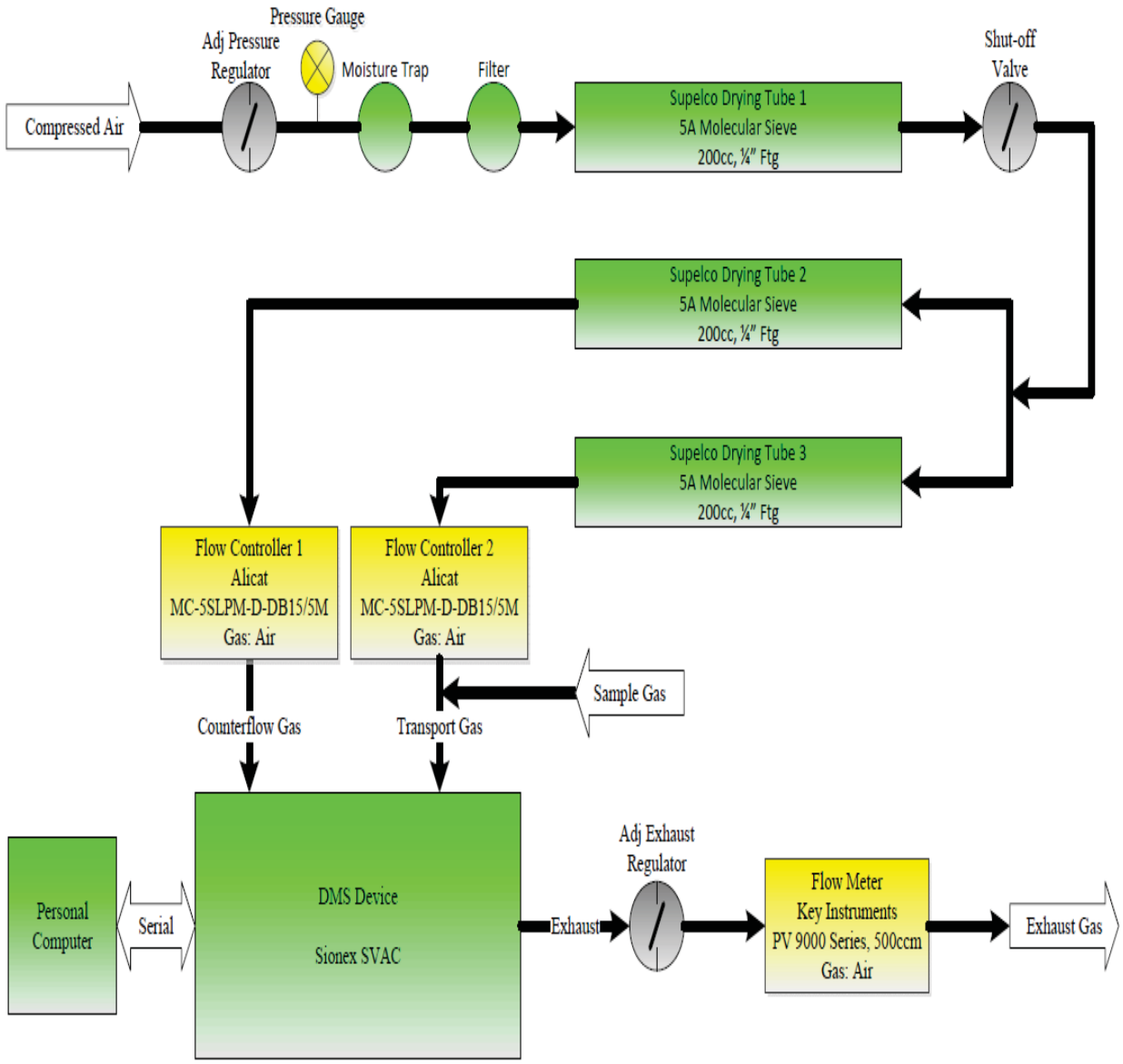

Figure 6 DMS Test Setup Architecture

Figure 6 is an architectural block diagram of the DMS test setup used for testing of the fatty acid samples. The specifics of each component used in the setup are described below.

1. Compressed Air: atmospheric air compressed with a commercial air compressor.
2. Adjustable Pressure Regulator: regulates incoming air pressure. Adjusted to 40 psi as indicated on the pressure gauge.
3. Pressure Gauge: indicator used for incoming compressed air adjustment.
4. Moisture Trap: Arrow Pneumatics DFD-10 Miniature In-Line Desiccant Dryer.
5. Filter: Norgren Excelon F72C-2AD-QL0 Oil Removal Filter (Coalescing) with 0.01um particulate removal to prevent impurities from entering subsequent components. Filter element part number 5925-09.
6. Supelco Drying Tubes 1, 2 and 3: Molecular Sieve 5A Moisture Trap, 200cc, Sigma-Aldrich PN 20618. Used to purify incoming air, prevent moisture and impurities larger than 5 Angstroms in diameter from passing through into the DMS instrument.
7. Flow Controller 1 and 2: Alicat MC-5SLPM-D-DB15/5M calibrated for air. Precisely regulates the flow rate of purified air for the Counterflow Gas and Transport Gas, respectively.
8. DMS Device: Sionex SVAC instrument retrofitted with the NRIS as the ion source. Powered from a 12VDC, 5A power supply.
9. Adjustable Exhaust Regulator: Manually adjustable valve used to regulate the flow rate of unwanted ions leaving the instrument. Flow rate adjusted to (40 sccm) as indicated on the flow meter.
10. Flow Meter: Key Instruments PV 9000 Series, 500 sccm calibrated for air.

11. Sample Introduction: The fatty acids were sampled using a gas tight 500uL glass syringe with 2 inch 22 gauge needle tip, Hamilton Company PN 81265 (Model 1750 RN, SYR). The samples were then introduced into the transport gas by inserting the needle tip through a septum in-line with the sample transport gas stream.

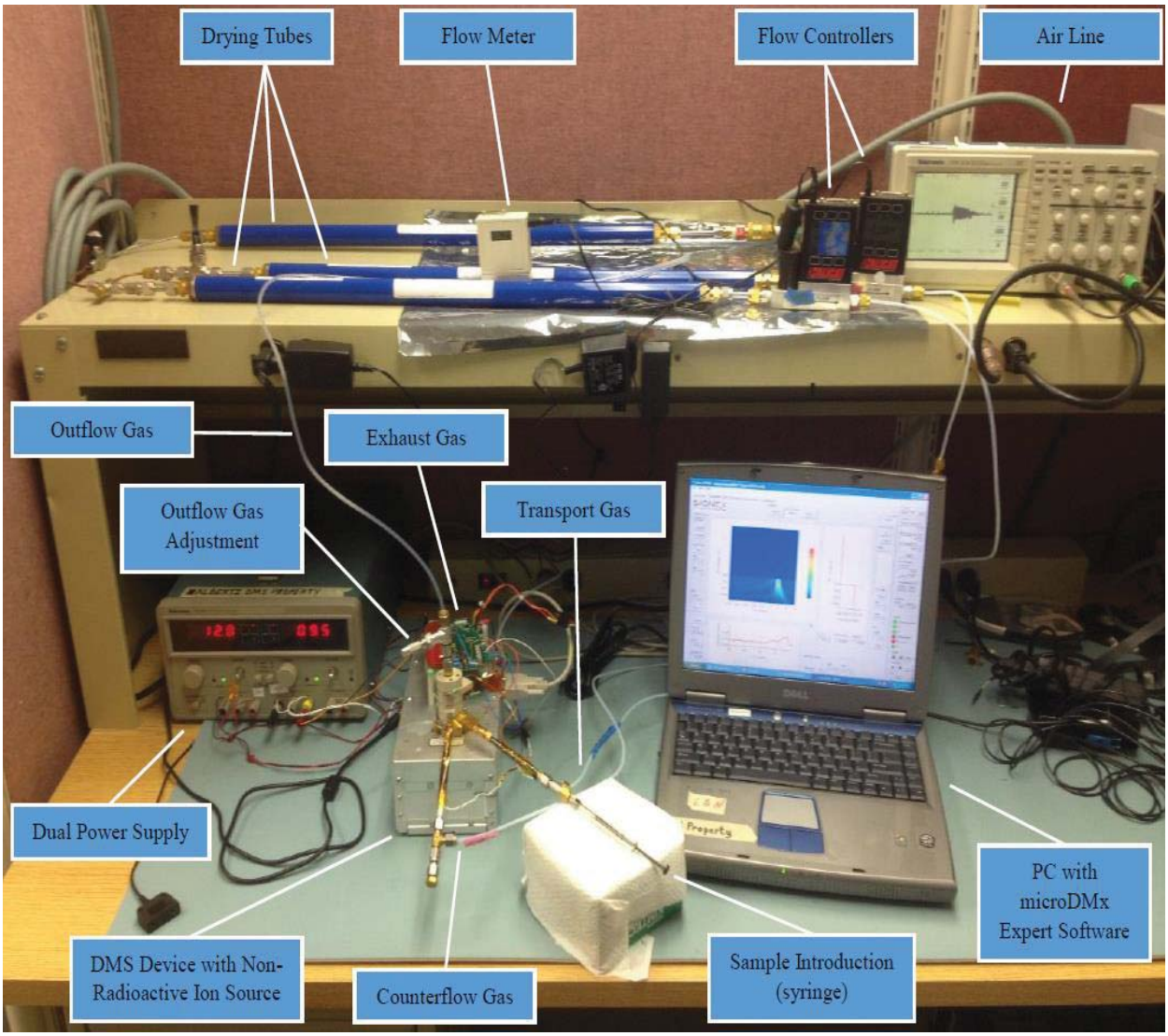

Figure 7 DMS Test Lab Setup

3.2. Test Samples

The fatty acid samples used for testing were purchased from the following suppliers:

- Linoleic Acid
    - Supplier: Abcam
    - Part Number: ab141144
    - Sample Size: 1 gram
    - Purity: > 99%
- Palmitic Acid
    - Supplier: Sigma-Aldrich
    - Part Number: P0500-25G
    - Sample Size: 25 grams
    - Purity: $\geq$ 99%
- Stearic Acid
    - Supplier: Sigma-Aldrich
    - Part Number: S4751-5G
    - Sample Size: 5 grams
    - Purity: Grade I, $\geq$ 98.5%

3.3. Test Method

Fatty acid testing was conducted over multiple days and before the start of each day of testing, the DMS instrument was run without sample for several days prior to allow clean air to travel through the system and exhaust contaminants introduced during assembly and previous sample testing. Resistive heaters wrapped around the stainless steel counterflow and transport gas

inlet tubes heat the incoming air to approximately 50°C to assist in dehydrating the air lines between the drying tubes and inlets.

At the start of each day of testing, prior to fatty acid sample introduction, dispersion plots were run in both the negative and positive ion modes, which recorded remaining contaminants in the system for identification from introduced samples. Baseline 2-D graphs were generated from the dispersion plots, with the pre-sample glass syringes inserted into the DMS, to ensure no contaminants were introduced by the syringes and mistaken for fatty acid sample response. These baseline graphs are used for comparison with fatty acid response in the 2-D graphs of Chapter 4.

The electric field across the NRIS and ionization chamber was adjusted to approximately 133V/cm, with the field pointing away from the DMS planar electrodes for the negative ion mode and into the planar electrodes for the positive ion mode.

To accurately control sample temperatures, the fatty acids were placed in 1 Dram borosilicate glass vials with solid top cap and PTFE/F217 Septa and placed in a controlled temperature water bath for 1 hour minimum at each sample temperature prior to introduction into the DMS. Water temperature was monitored using a NIST traceable digital temperature sensor, Fisher Scientific PN S90862, with +/- 1°C accuracy.

Atmospheric pressure was measured using a NIST certified digital barometer obtained from The Weather Store, part number 1081. Its barometric range is 600 to 787.6 mmHg (800 to 1050 mbar) with a resolution of 1.6 mmHg (1 mbar). Accuracy is +/- 4.5 mmHg (+/- 6 mbar) from 667.6 to 765.1 mmHg (890 to 1020 mbar), otherwise +/- 7.5 mmHg (+/- 10 mbar).

After a 1 hour minimum water bath dwell time at the programmed sample temperature, +/- 1°C of the sample target temperature, a fatty acid gas sample was extracted from the glass vial using the pre-sample glass syringe baselined in the DMS prior to the start of testing. The gas

sample was extracted from the headspace above the fatty acid. A separate glass syringe was used for each of the three fatty acids to prevent cross-contamination and the same glass syringe was used for all samples of the same fatty acid. The syringes were preheated to approximately the same temperature as the inlet surface temperatures, prior to sample extraction.

The needle tip of the syringe was inserted through a septum into the transport gas inlet and a controlled volume of gas injected into the stream using the graduated microliter (uL) markings on the syringe glass surface.

The Sionex DMS application software, microDMx Expert, was used to control instrument operation including RF voltage, Compensation voltage, sampling time, step size, etc. Generated data was saved in Microsoft Excel file format via the application software. Igor Pro 6.11 was used for post processing of the DMS generated Excel data to create the graphs and plots shown in Chapter 4: Experimental Results.

The sample response time was measured using a stopwatch with 0.01 second resolution. Times measured are from sample introduction to initial detection and to peak signal intensity level.

3.4. Graphical Representation of Data

Test sample response generated by the DMS instrument will be displayed using a Dispersion Plot, which graphs test data using both 3-D and 2-D linear graphs, as shown in Figure 8. The Dispersion Plots show the 3-D response for both positive and negative ion scans (left and right panels, respectively) over the RF voltage scan range (left Y-axis (1)) versus the x-axis compensation voltage scan range (2). Gas ions detected by the DMS instrument are revealed by shape and color changes shown in the 3-D graphs. Detected ions of a particular gas will typically have a unique shape compared to ions of other gasses, however, ions of the same gas will have the same shape. Concentration changes are revealed by changes in signal intensity, represented by

color variances in the 3-D plots. Also, positive ions versus negative ions of the same gas can have unique shapes but will be consistent in shape for the same ion polarity over multiple samples of the same gas. A gas may show a response only for positive ions, negative ions or both.

Comparing dispersion plots of different gasses for a particular ion polarity (positive or negative) and identifying the RF and compensation voltages where differences occur allows the gas to be uniquely identified. If gas ions are from a similar chemical family, such as the fatty acids used in this testing, the shapes can be very similar but have slight differences in the curvature of the shape as the RF and compensation voltages are scanned throughout their range. The goal is to identify unique compensation voltage (Vc) values for each species of gas ions at one or more RF voltages in either negative, positive or both ion polarities. The unique Vc value is what allows filtering and differentiation of the gas ions in the DMS instrument.

The color scale (3) in Figure 8 shows the numerical intensity level associated with a particular color in the 3-D plots as the RF and Compensation voltages are scanned through their defined ranges. Numerical intensity scales are also shown in the x-axis to the left and right of the 3-D panels (4) and represent the signal response at a specific compensation voltage value over the full RF voltage range. The compensation voltage value shown in Figure 8 is chosen at Vc = -1.14V and is displayed in the box at the upper left of the figure (6), represented by the vertical dashed line shown in the 3-D plots. The compensation voltage is chosen by adjusting sliders in the data software and selecting a value within the compensation voltage scan range of -30V to +10V.

Signal intensity scales are also shown in the Y-axis on the left (Positive ion scan) and right (Negative ion scan) of the 2-D plots (5), at the bottom of the figure, and represent the signal response at a specified RF voltage over the compensation voltage scan range. The specified RF voltage shown in Figure 8 is chosen at RF = 700V (7), also represented by the horizontal dashed

line shown in the 3-D plots. The displayed RF voltage is chosen by adjusting sliders in the data software and selecting a value within the RF voltage scan range of +500V to +1350V.

The numerical values for signal intensity represent amplified voltages of the measured signal on the Ion Detector plates with a Gain = 12,570. For a signal intensity value = 0.100V, this corresponds to an ion detector plate voltage of 7.96uV (0.100V / 12,570).

The RF and Compensation voltages chosen for display in the 2-D linear plots of subsequent figures in Chapter 4: Experimental Results, will be selected to show where the DMS signal response of the fatty acids are maximized and the system contaminants are minimized per the results derived from the 3-D plots of each fatty acid sample.

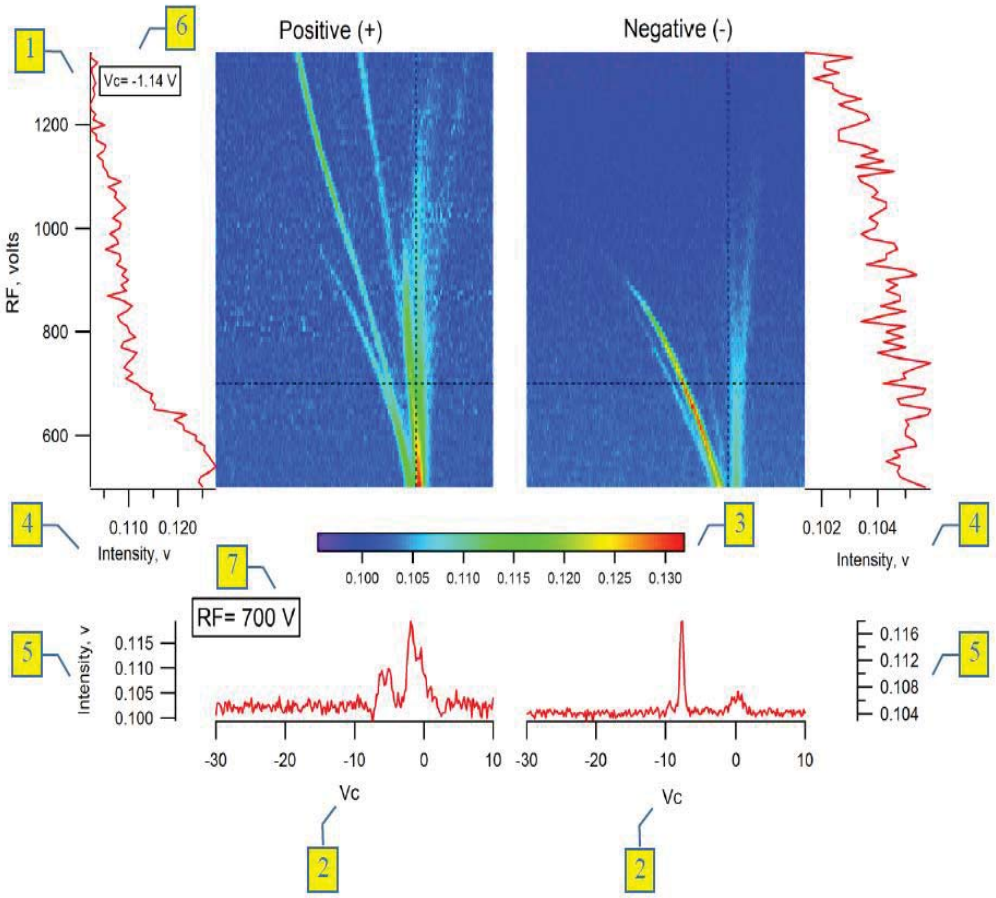

Figure 8 DMS Dispersion Plot

CHAPTER 4: EXPERIMENTAL RESULTS

4.1. DMS and Test Setup Adjustments

Table 2 lists the DMS and test setup adjustments used in all testing.

Table 2 DMS and Test Setup Adjustments for all Testing

PARAMETER	VALUE
Counterflow gas in (flow controller 1)	purified air at 150 sccm flow rate
Transport gas in (flow controller 2)	purified air at 550 sccm flow rate
Outflow gas (flow meter)	41 sccm outflow rate
Dispersion Plot DMS RF Voltage Range	500V to 1350V in 10V increments
Dispersion Plot DMS Compensation Voltage Range	-30V to +10V in 0.183V increments

4.2. Baseline DMS Measurements

4.2.1. Environmental Condition and Test Gas Information

Theoretical headspace saturation concentration is calculated using published vapor pressure data for the chemical and measured Barometric Pressure, per formula [24]:

$$\text{ppm} = \frac{\text{Vapor Pressure Chemical (mmHg)}}{\text{Barometric Pressure (mmHg)}} \text{ x } 10^6 \quad (4)$$

Table 3 lists the environmental condition present during baseline testing and the chemical information for Methyl Salicylate (MS), which is the test gas that was used to verify DMS functionality prior to the start of fatty acid testing. For MS, the headspace concentration = 44.89 ppm at 25°C.

Table 3 Baseline Measurements Environmental Condition and MS Information

CONDITION	VALUE
Date, Time	01/07/2017, 2:13pm
Barometric Pressure	764.032 mmHg
Room Temperature	23.3°C (74°F)
Formula [25]	$C_8H_8O_3$
Molar Mass [25]	152.149 g/mol
Melting Point [25]	-8.6°C (16.5°F)
Flash Point (closed cup) [25]	96°C (204.8°F)
Boiling Point [25]	222°C (431.6°F)
Vapor Pressure [25]	0.0343 mmHg at 25°C

4.2.2. System Contaminants and Background Response

A dispersion plot for both the positive and negative ion modes, prior to the introduction of any samples or syringes, was generated to determine any existing contaminants and background response within the system so that they can be distinguished from the signal response of subsequent plots during fatty acid testing. Figure 9 shows the dispersion plot of the DMS contaminant response. As can be seen from the 3-D negative plot, RF voltages above approximately 1000V show little to no contamination or background response. The 3-D positive plot shows reduced contaminant and background response at RF voltages above 1000V.

Some of the contaminants in the system include ions from the material making up the system such as the PEEK material forming the ionization chamber and the ceramic housing of the DMS electrodes. Also, trace amounts of previous gas samples may contribute to the contaminants,

however, this is minimized by allowing filtered air to run through the system for several days prior to start of testing for each fatty acid. The background response is formed primarily by components of air, including nitrogen, oxygen and water vapor, which when colliding with ions formed by plasma, also become ionized and respond to the RF and compensation voltages in the DMS system.

The dispersion plot shown in Figure 10 was generated with a glass syringe inserted into the DMS transport gas inlet prior to sampling the Stearic acid to ensure that DMS response during sampling is due to introduced chemical and not impurities in the syringe. Comparing dispersion plot Figures 9 and 10 show little difference, confirming that the syringe does not introduce additional contaminants into the system. This was consistent for all glass syringes used for testing.

4.2.3. Verification of DMS Functionality

Figure 11 is the response for 10uL of Methyl Salicylate (MS) in the DMS system at a room temperature of 23°C. The dispersion plot for MS is generated prior to the start of fatty acid testing and compared with the expected Compensation Voltage response obtained in tests from prior work with this chemical. Its high vapor pressure of 0.0343 mmHg at 25°C provides a strong response to the DMS and dissipates quickly when the sample is removed from the instrument. As can be seen from the 3-D graph, the signal intensity of MS at room temperature is significantly greater than the contaminant response shown in Figures 9 and 10, such that the contaminants are not visible in the MS dispersion plot. The adjusted signal intensity range is shown in the color scale beneath the 3-D graphs of Figure 11. Figure 12 shows that the contaminant signal response returns to its pre-Methyl Salicylate levels once the sample is removed. All baseline measurements made prior to the start of each fatty acid testing are comparable to the response shown in Figure 12.

Because the fatty acids under test have significantly lower vapor pressures than MS, the concentration of target gas molecules in the headspace above the chemicals will be lower and the

resulting signal intensities are expected to be less than MS. Fatty acid response will be investigated at RF voltages of 1000V or greater where there is increased probability of differentiation without interference from system contaminants.

Figures 13 and 14 are 2-D graphs showing the Signal Intensity versus Compensation Voltage (Vc) for the test setup conditions shown in Figures 9, 10, 11 and 12, at an RF voltage (Vrf) = 1330V, for both the negative and positive ion modes, respectively. For the negative ion mode, Methyl Salicylate peaks occur at Vc = -7.35V and -3.15V. For the positive ion mode, the Methyl Salicylate peak occurs at -3.33V, with contaminant response (two smaller peaks) occurring at Vc = -9.36V and -18.13V. The background noise level of the instrument is 0.102V for both polarities. Referencing Figures 13 and 14, the equation for the signal to noise ratio (SNR) is,

$$SNR = S / N \tag{5}$$

where N is the peak to peak noise for the baseline measurement (not including contaminant responses) and S is measured from the baseline noise average to the peak signal response. The limit of detection for signal intensity response will be chosen at 3N. Values with a SNR $\geq$ 3 will be considered a valid response for all samples. The SNR values for Methyl Salicylate are listed below:

- SNR_{MS-} = (0.116100V – 0.102V) / 0.001476V) = 9.55 Major Peak
- SNR_{MS-} = (0.105373V – 0.102V) / 0.001476V) = 2.29 Minor Peak (SNR < 3)
- SNR_{MS+} = (0.133552V – 0.102V / 0.003514V) = 9

where noise peak to peak N = 0.001476V for the negative ion mode and N = 0.003514V for the positive ion mode.

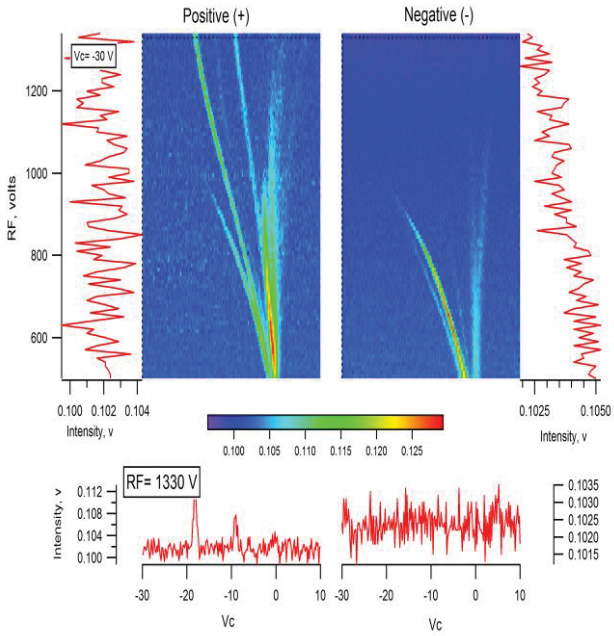

Figure 9 Background DMS Noise (No Sample)

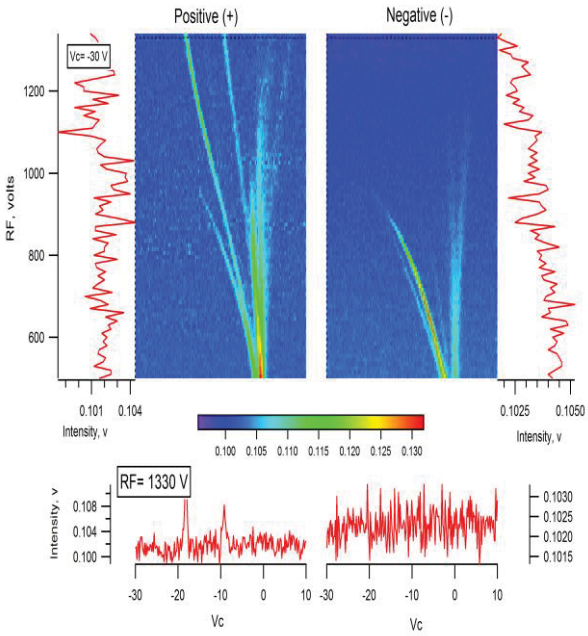

Figure 10 Pre-Sample Syringe in DMS

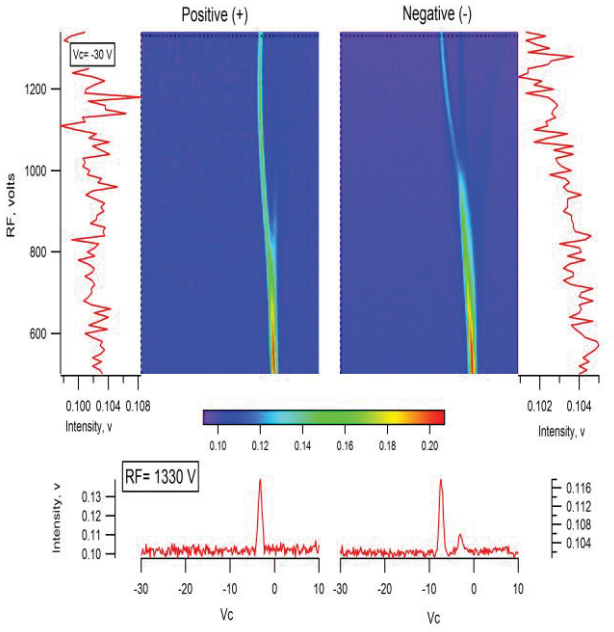

Figure 11 Methyl Salicylate, 10uL

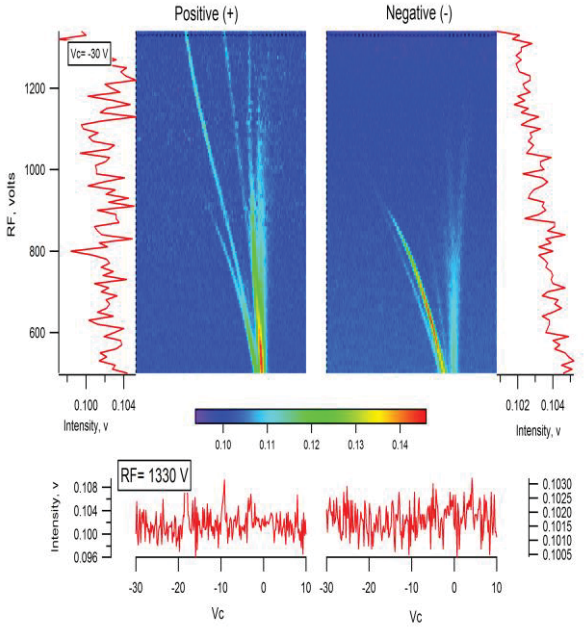

Figure 12 Pre-Sample Syringe after Methyl Salicylate (Baseline)

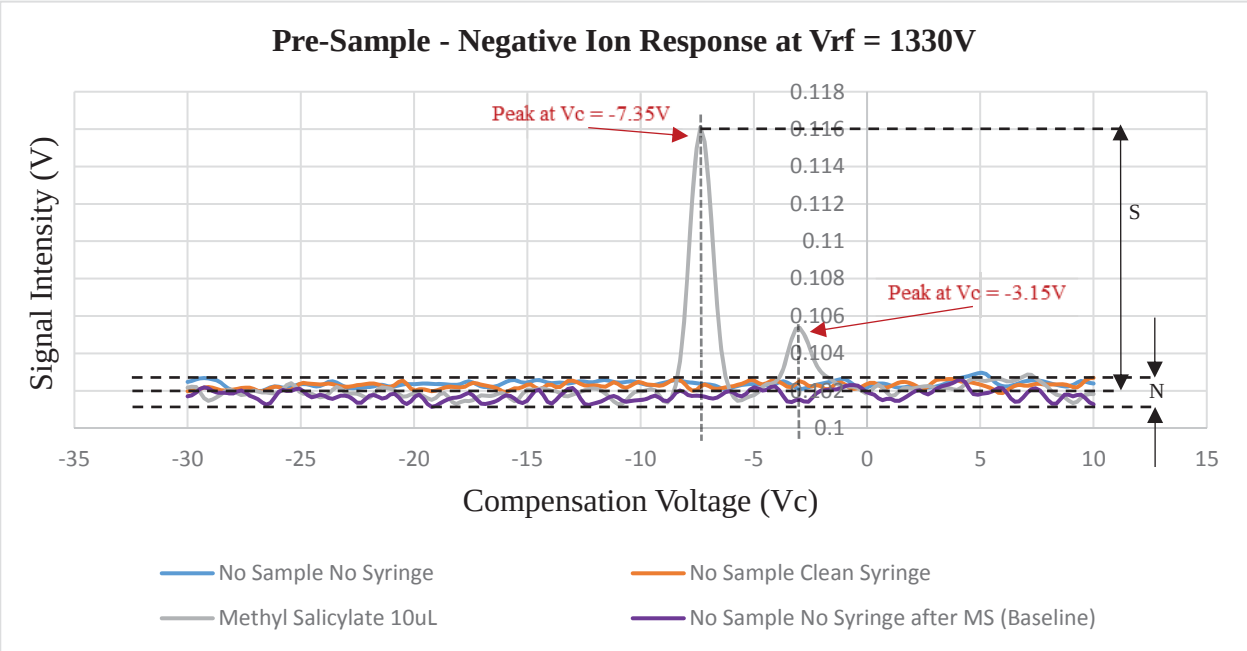

Figure 13 Pre-Sample - Negative Ion Response at Vrf = 1330V

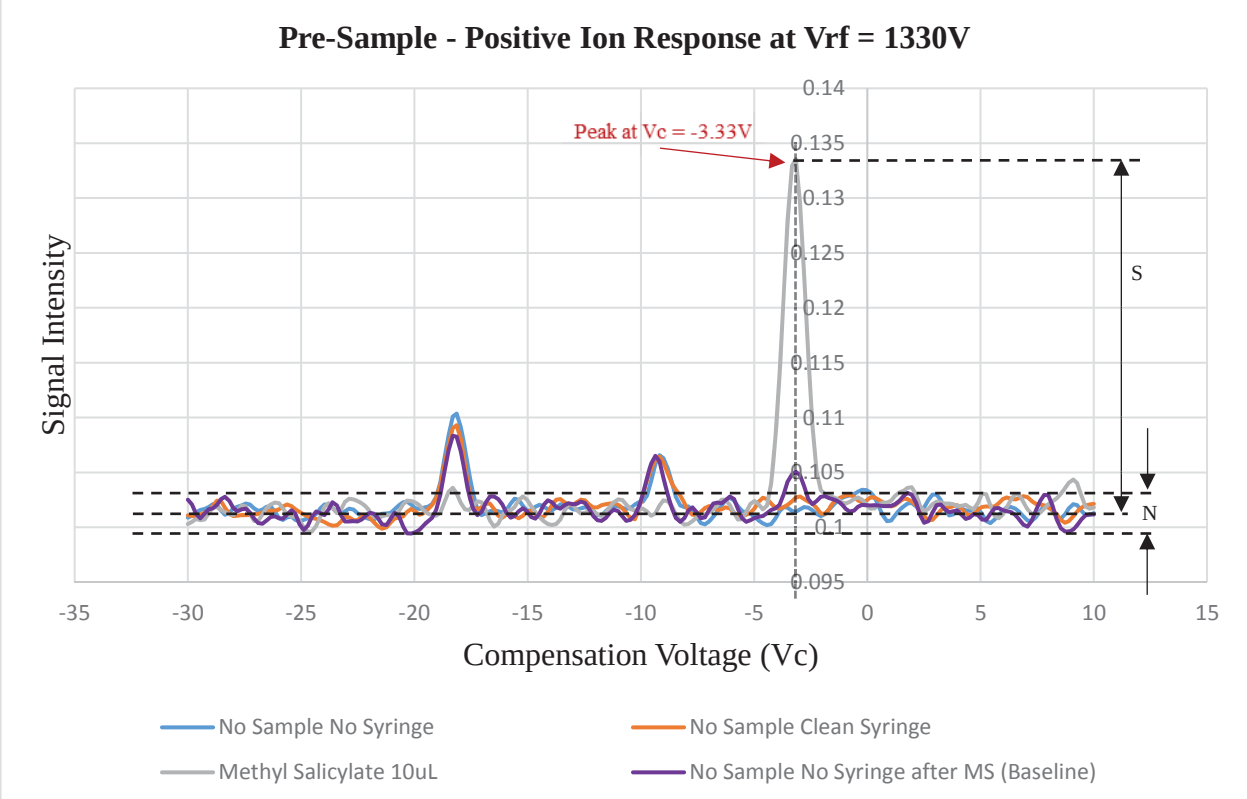

Figure 14 Pre-Sample - Positive Ion Response at Vrf = 1330V

4.3. Stearic Acid

4.3.1. Stearic Acid Environmental Condition and Chemical Information

Table 4 lists the environmental condition present during Stearic acid testing and its chemical information. Entering the pressure information into equation 4, the headspace saturation concentration for Stearic acid at 25°C is calculated to be:

$$\text{Concentration of Stearic Acid @ } 25°C = \frac{4.28 \text{ x } 10^{-8} \text{mmHg}}{770.128 \text{ mmHg}} \text{ x } 10^{6} = 55.6\, x10^{-6} \text{ ppm} \quad (6)$$

Table 4 Stearic Acid Testing Environmental Condition and Chemical Information

CONDITION	VALUE
Date, Time	01/07/2017, 4:00 pm; 25°C, 60°C, 70°C testing 01/14/2017, 12:15pm; 75°C testing
Barometric Pressure	01/07/2017, 4:00 pm; 764.032 mmHg 01/14/2017, 12:15pm; 770.128 mmHg
Room Temperature	01/07/2017, 4:00 pm; 23.3°C (74°F) 01/14/2017, 12:15pm; 22.8°C (73°F)
Formula [26]	$C_{18}H_{36}O_2$
Molar Mass [26]	284.484 g/mol
Melting Point [26]	69.3°C (156.7°F)
Flash Point (closed cup) [26]	196.1°C (385°F)
Boiling Point [26]	350°C (662°F)
Vapor Pressure [26]	4.28 x 10^{-8} mmHg at 25°C

4.3.2. Stearic Acid Dispersion Plot

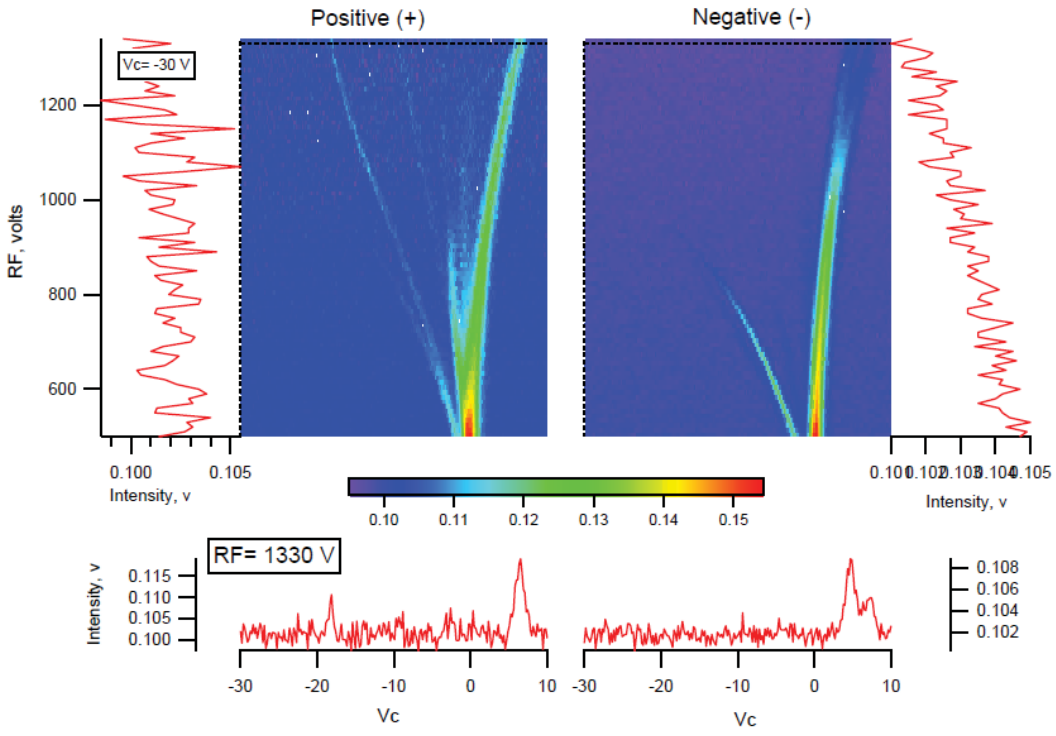

Figure 15 Stearic Acid 75°C 30uL, Vrf Slider Set to 1330V

Stearic acid samples were tested at 25°C, 60°C, 70°C and 75°C. The strongest response across the RF scan range was obtained at a sample temperature of 75°C for a 30uL volume, and is shown in the dispersion plot of Figure 15. Figures 16 and 17 show the Intensity versus Compensation Voltage response of Stearic acid at an RF voltage of 1330V for all sample temperatures in the negative and positive ion modes, respectively. A RF voltage of 1330V was chosen for the 2-D graphs because it is the voltage that shows peak separation between Stearic acid and the other fatty acids as determined by a comparison of the dispersion plots.

No response was obtained at 25°C and 60°C for either ion polarity since Stearic acid is a solid at these temperatures with very low vapor pressure and doesn't transform into a liquid until reaching its melting point temperature of 69.3°C. Vapor pressure increases non-linearly with rising

temperature allowing a greater concentration of gas molecules to exist in the headspace above the acid and increasing the probability of detection.

For the negative ion mode, no differentiation from the baseline response was obtained for the 70°C 200uL and 300uL samples. A small differentiation from the baseline intensity response was obtained for the 70°C 100uL and 75°C 1uL volumes, however, the SNR for these samples is less than 3 and cannot be considered reliable indicators of detection. Good signal intensity response was obtained for the 75°C 10uL, 30uL and 50uL volumes, as shown in Figure 18, each having a SNR greater than 3. The major peaks align at a compensation voltage of 4.70V. A minor peak is observed at a compensation voltage of 7.26V and, despite having signal intensity levels less than 3, the waveform shape and location of the minor peak compensation voltage can be used in combination with the major peak information for acid identification. Minor peaks occur when the gas sample combines with ions of a different negative charge than the major peak ions, causing the molecule to respond at a different compensation voltage value. Because these interactions occur at a lower frequency than the major peak ions, the resulting signal intensity is lower. Table 5 lists the compensation voltage, signal intensity and SNR for each response curve in Figure 18.

Table 5 Stearic Acid Negative Ion Compensation Voltage at Peak Signal Intensity

TEMPERATURE	VOLUME	COMPENSATION VOLTAGE (Volts) Major Peaks	SIGNAL INTENSITY (Volts) Major Peaks	SNR Major Peaks	COMPENSATION VOLTAGE (Volts) Minor Peaks
	Baseline (Average)		0.102000		
75°C	10uL	4.70	0.106806	3.26	7.26
	30uL	4.70	0.108120	4.15	7.26
	50uL	4.70	0.107820	3.94	7.26
Median		4.70	0.107820	3.94	7.26
Average (Tolerance)		4.70	0.107583 (+0.0005/-0.0008)	3.78 (+0.37/-0.52)	7.26

For the positive ion mode, no differentiation from the baseline response was obtained for the 25°C, 60°C and 70°C samples. A small differentiation from the baseline intensity response was obtained for the 75°C 1uL and 10uL volumes, however, the SNR for these values is less than 3 and cannot be considered reliable indicators of detection. Good signal intensity response was obtained for the 75°C 30uL and 50uL volumes, as shown in Figure 19, each having a SNR greater than 3. The 30uL and 50uL major peaks are located at compensation voltages of 6.53V and 6.71V, respectively. The Stearic acid curves also have three minor peaks in the negative region of the compensation voltage but do not differentiate from the baseline curve and cannot be used for acid identification. Table 6 lists the compensation voltage, signal intensity and SNR for each response curve in Figure 19.

Table 6 Stearic Acid Positive Ion Compensation Voltage at Peak Signal Intensity

TEMPERATURE	VOLUME	COMPENSATION VOLTAGE (Volts) Major Peaks	SIGNAL INTENSITY (Volts) Major Peaks	SNR Major Peaks
	Baseline (Average)		0.102000	
75°C	30uL	6.53	0.119000	4.84
	50uL	6.71	0.114886	3.67
Median		6.62	0.116943	4.26
Average (Tolerance)		6.62	0.116943 (+/- 0.002)	4.26 (+/- 0.59)

The measured response times of the 75°C 30uL sample are as follows:

- Sample introduction to initial detection = 2.21 seconds
- Sample introduction to peak intensity = 7.51 seconds

Upon removal of the sample, several minutes are required for the intensity level to decrease from its peak level.

4.3.3. Stearic Acid Sample Results at Vrf = 1330V

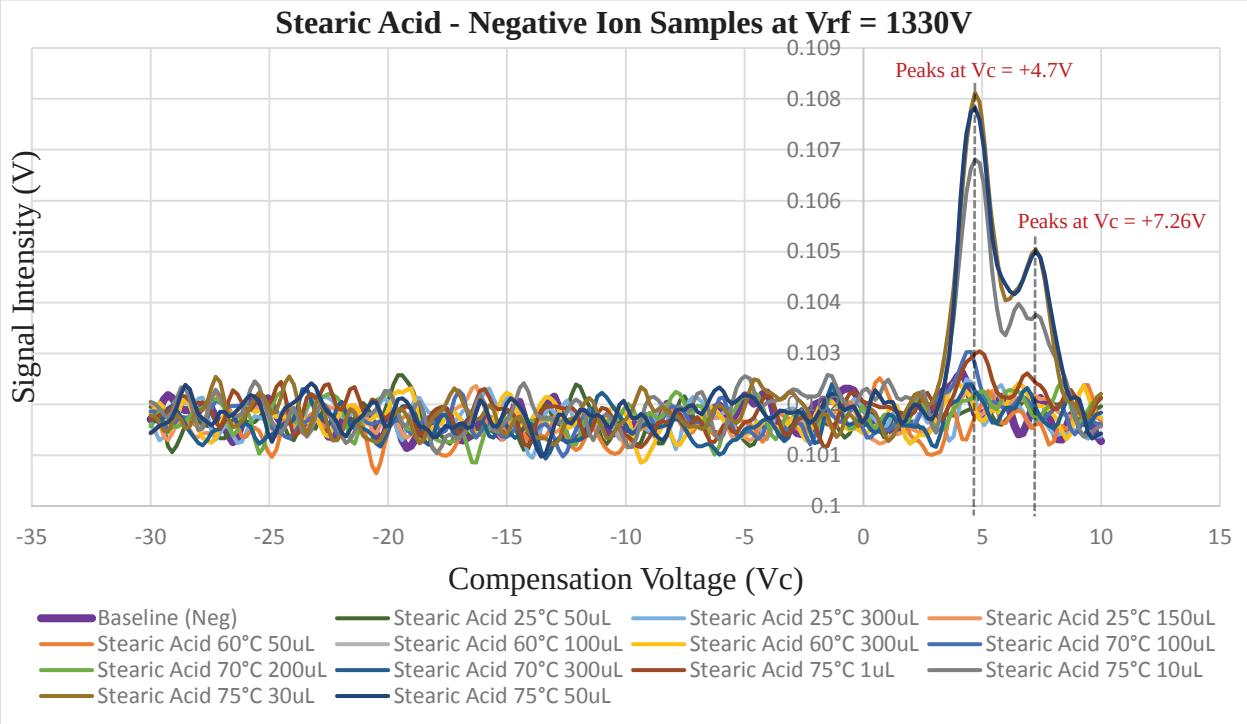

Figure 16 Stearic Acid - Negative Ion Samples at Vrf = 1330V

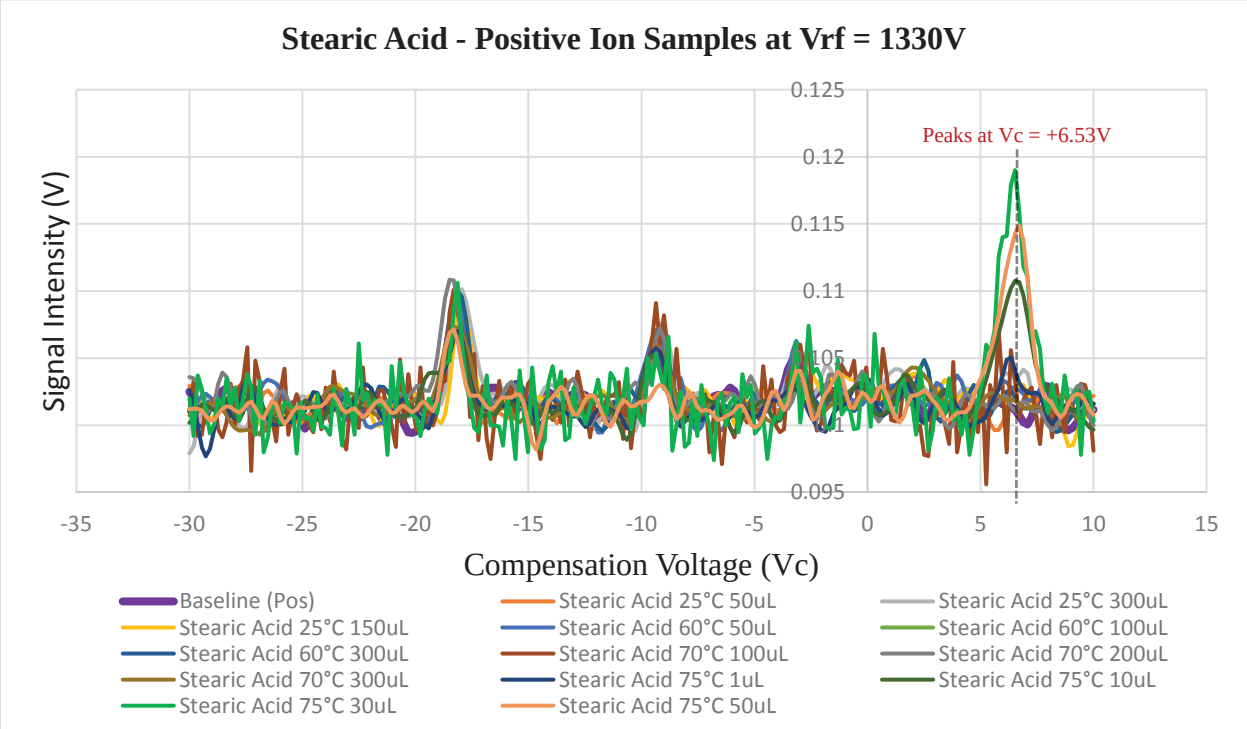

Figure 17 Stearic Acid - Positive Ion Samples at Vrf = 1330V

4.3.4. Stearic Acid Sample Results with Response at Vrf = 1330V

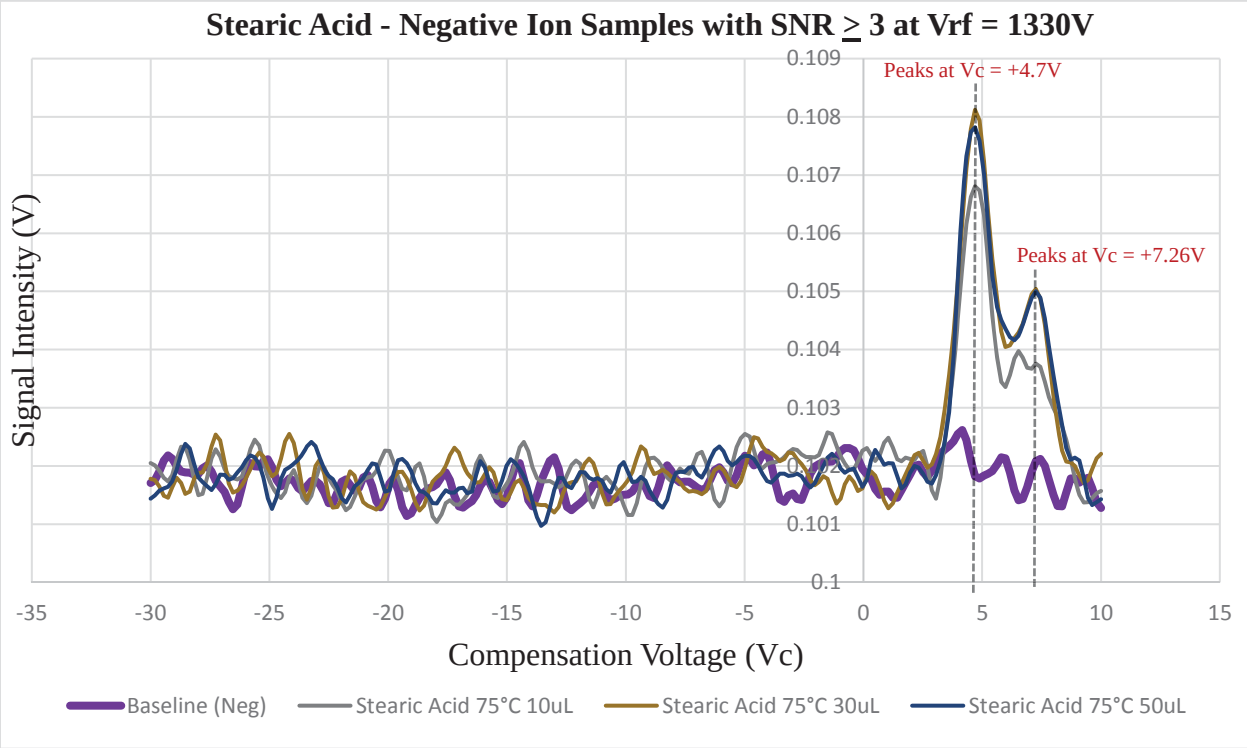

Figure 18 Stearic Acid - Negative Ion Samples with SNR ≥ 3 at Vrf = 1330V

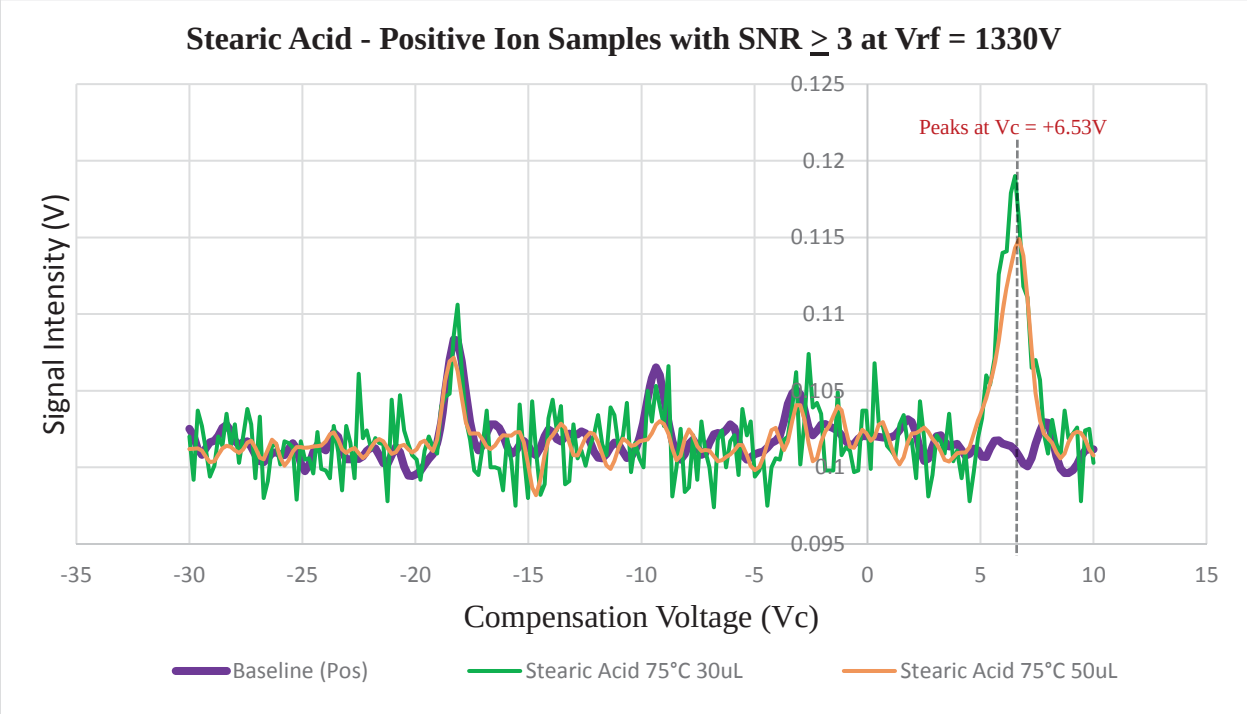

Figure 19 Stearic Acid - Positive Ion Samples with SNR ≥ 3 at Vrf = 1330V

4.4. Palmitic Acid

4.4.1. Palmitic Acid Environmental Condition and Chemical Information

Table 7 lists the environmental condition present during Palmitic acid testing and its chemical information. Entering the pressure information into equation 4, the headspace saturation concentration for Palmitic acid at 25°C is calculated to be:

$$\text{Concentration of Palmitic Acid @ 25°C} = \frac{3.8 \times 10^{-7}\text{mmHg}}{756.666\ \text{mmHg}} \times 10^{6} = 502.2\ x10^{-6}\ \text{ppm} \quad (7)$$

Table 7 Palmitic Acid Testing Environmental Condition and Chemical Information

CONDITION	VALUE
Date, Time	01/21/2017, 2:00 pm; 25°C, 60°C, 70°C testing 02/17/2017, 7:00pm; 75°C testing
Barometric Pressure	01/21/2017, 2:00 pm; 756.666 mmHg 02/17/2017, 7:00pm; 761.746 mmHg
Room Temperature	01/21/2017, 2:00 pm; 22.8°C (73°F) 02/17/2017, 7:00pm; 23.3°C (74°F)
Formula [27]	$C_{16}H_{32}O_2$
Molar Mass [27]	256.43 g/mol
Melting Point [27]	62.5°C (144.5°F)
Flash Point [28]	113°C (235.4°F)
Boiling Point [27]	351.5°C (664.7°F)
Vapor Pressure [27]	3.8 x 10^{-7} mmHg at 25°C

4.4.2. Palmitic Acid Dispersion Plot

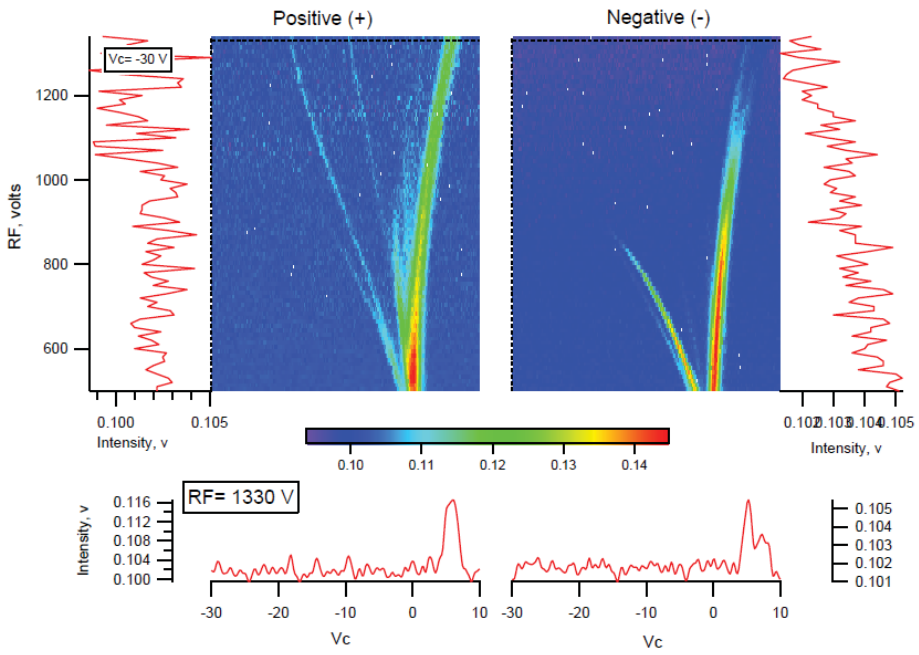

Figure 20 Palmitic Acid 70°C 50uL, Vrf Slider Set to 1330V

Palmitic acid samples were tested at 25°C, 60°C, 70°C and 75°C temperatures. The strongest response across the RF scan range was obtained at a sample temperature of 70°C for a 50uL volume and is shown in the dispersion plot of Figure 20. Figures 21 and 22 show the Intensity versus Compensation Voltage response of Palmitic acid at an RF voltage of 1330V for all sample temperatures in the negative and positive ion modes, respectively. As mentioned previously, a RF voltage of 1330V was chosen for the 2-D graphs because it is the voltage that shows some peak separation between the other fatty acids.

The 75°C data in Figures 21 and 22 shows anomalous peaks inconsistent with the curves of the other samples at lower temperatures and is not included in the response graphs of Figures 23 and 24 due to suspected intermittent behavior of the plasma ion source on day 02/17/17 of testing. Only the 75°C data for Palmitic acid is suspect since all other temperature samples for the three fatty acids were taken on prior days when the plasma ion source was observed to be

functioning properly. Chapter 5: Discussion and Future Work describes in greater detail the observed intermittent behavior of the plasma ion source and the potential cause for the issue.

For the negative ion mode, no differentiation from the baseline response was obtained for the following samples: 25°C 50uL, 100uL, 70°C 50uL (first of three 50uL samples), 100uL (first of three 100uL samples). A small differentiation from the baseline intensity response was obtained at 25°C 150uL, and 60°C 50uL, 100uL, 150uL, 70°C 50uL (second of three 50uL samples), 100uL (second of two 100uL samples), 150uL volumes, however, the SNR for these samples is less than 3 and cannot be considered reliable indicators of detection. The strongest signal intensity response in the negative ion mode occurs for 70°C 50uL (third sample of three 50uL samples) with a SNR = 2.4, however, it is still below the required SNR level of 3 to be considered reliable for detection. As a result, the negative ion mode fails to provide reliable detection for Palmitic acid at the temperatures and volumes tested.

For the positive ion mode, no differentiation from the baseline response was obtained for the 25°C samples. Some differentiation from the baseline intensity response was obtained for the all the 60°C and 70°C volumes, however, except for the 70°C 50uL (third of three 50uL sample), the SNR for these volumes is less than 3 and cannot be considered reliable indicators of detection. Good signal intensity response was obtained for the 70°C 50uL (third of three 50uL samples) volume, as shown in Figure 23, having a SNR = 4.14. The 50uL major peak is located at a compensation voltages of 5.98V. The Palmitic acid curves have two minor peaks in the negative region of the compensation voltage but do not differentiate well from the baseline curve and cannot be used for acid identification. Table 8 lists the compensation voltage and signal intensity for the response curve in Figure 23.

Table 8 Palmitic Acid Positive Ion Compensation Voltage at Peak Signal Intensity

TEMPERATURE	VOLUME	COMPENSATION VOLTAGE (Volts) Major Peaks	SIGNAL INTENSITY (Volts) Major Peaks	SNR Major Peaks
	Baseline (Average)		0.102000	
75°C	50uL (3rd sample)	5.98	0.116548	4.14
Median		5.98	0.116548	4.14
Average (Tolerance)		5.98	0.116548	4.14

The measured response times of the 70°C 50uL (3rd sample) are as follows:

- Sample introduction to initial detection = 2.31 seconds
- Sample introduction to peak intensity = 34.47 seconds

Upon removal of the sample, several minutes are required for the intensity level to decrease from its peak level.

4.4.3. Palmitic Acid Sample Results at Vrf = 1330V

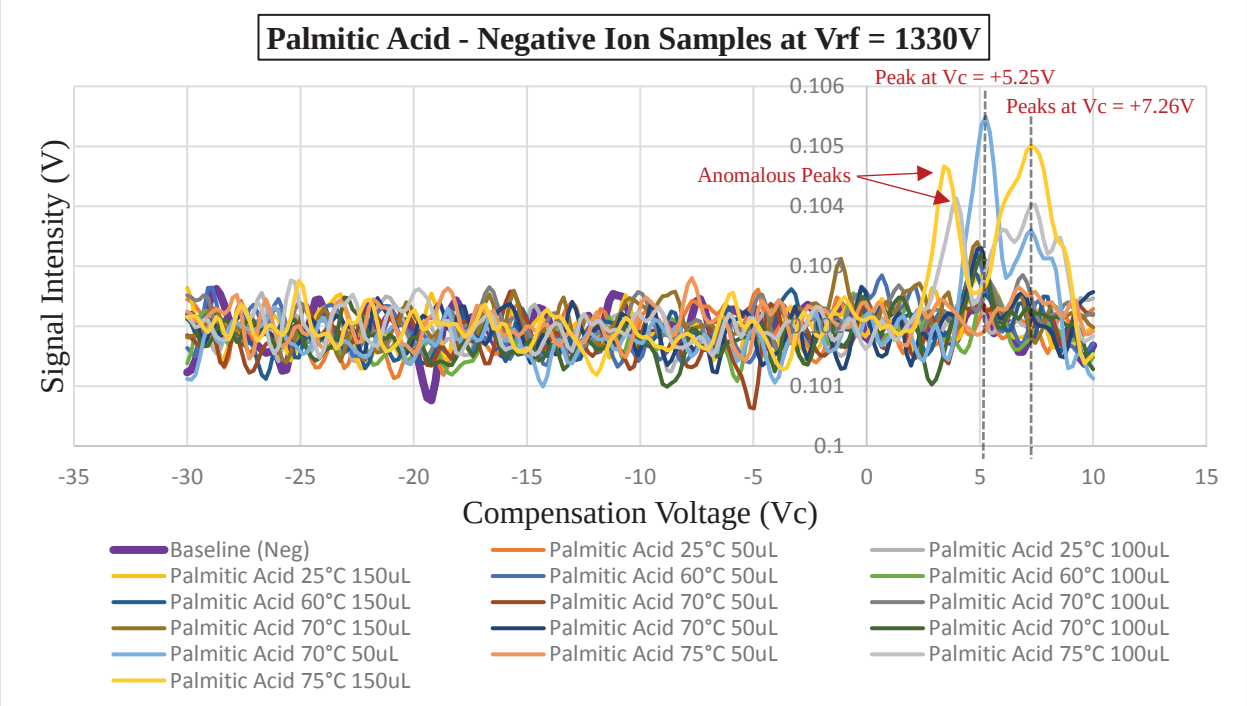

Figure 21 Palmitic Acid - Negative Ion Samples at Vrf = 1330V

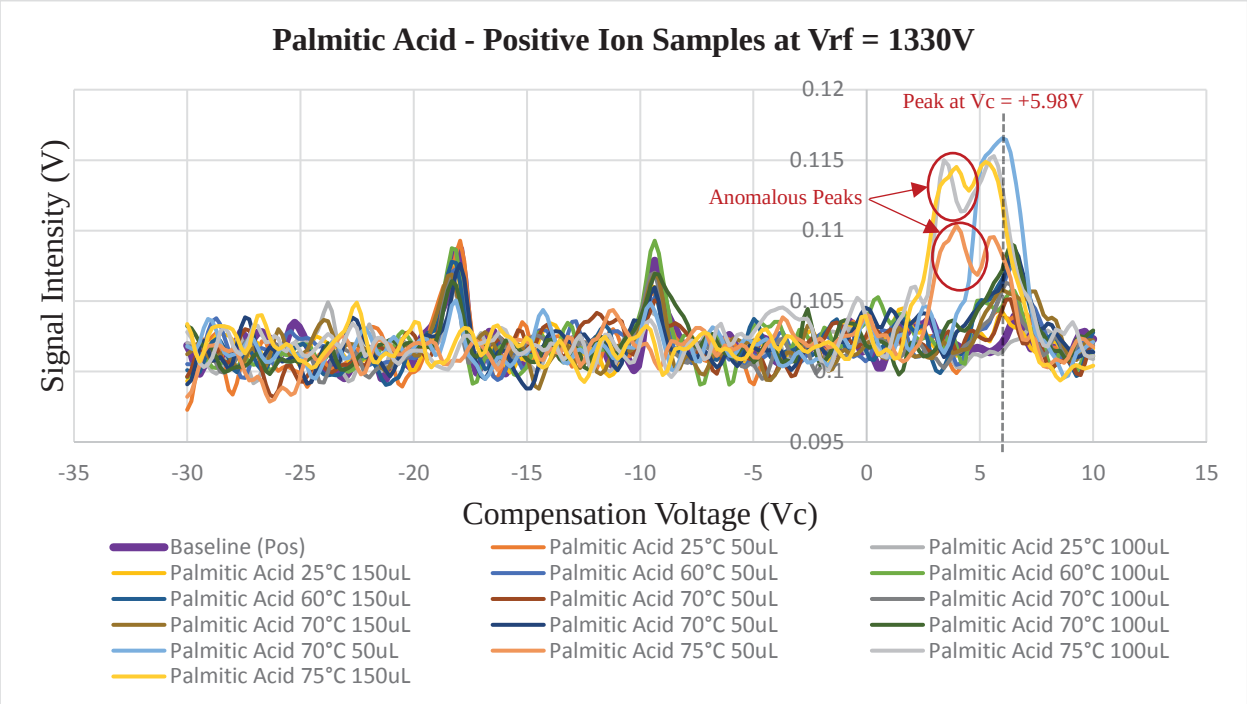

Figure 22 Palmitic Acid - Positive Ion Samples at Vrf = 1330V

4.4.4. Palmitic Acid Sample Results with Response at Vrf = 1330V

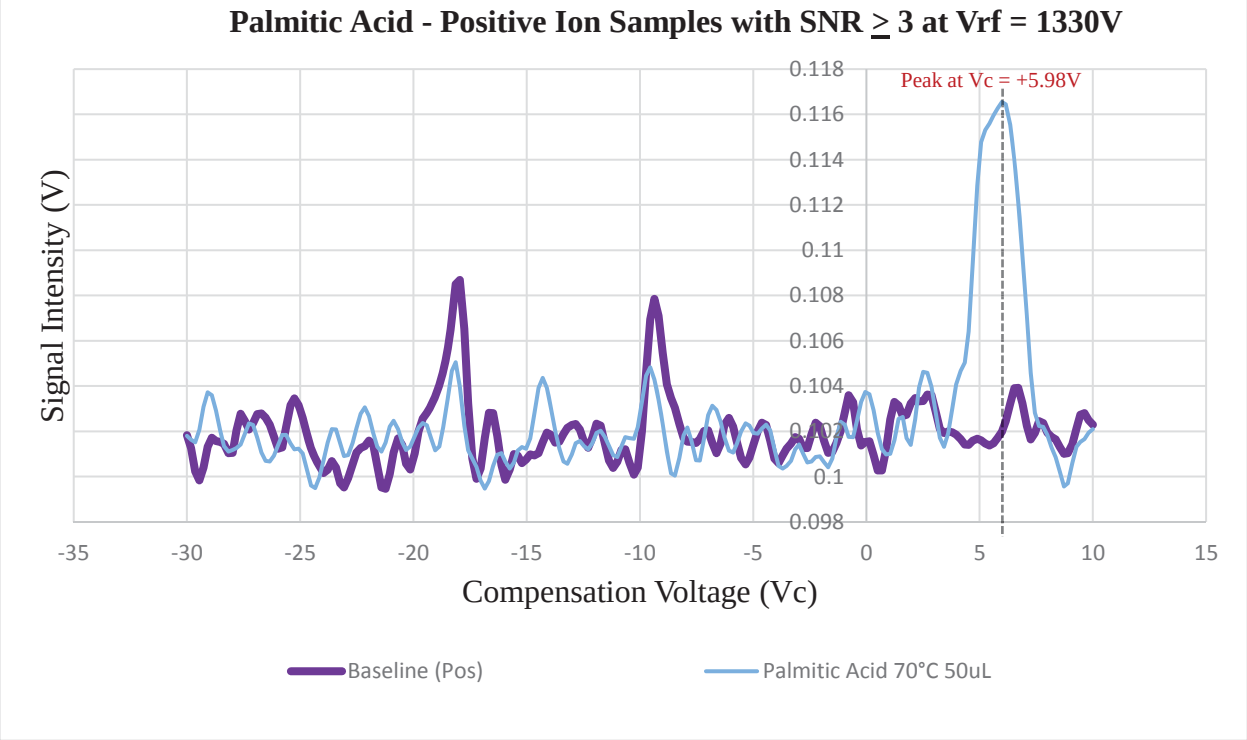

Figure 23 Palmitic Acid - Positive Ion Samples with SNR ≥ 3 at Vrf = 1330V

4.5. Linoleic Acid

4.5.1. Linoleic Acid Environmental Condition and Chemical Information

Table 9 lists the environmental condition present during Linoleic acid testing and its chemical information. Entering the pressure information into equation 4, the headspace saturation concentration for Linoleic acid at 25°C is calculated to be:

$$\text{Concentration of Linoleic Acid @ } 25°\text{C} = \frac{8.68 \text{ x } 10^{-7}\text{mmHg}}{763.270 \text{ mmHg}} \text{ x } 10^{6} = 1.142\, x10^{-3} \text{ ppm} \quad (8)$$

Table 9 Linoleic Acid Testing Environmental Condition and Chemical Information

CONDITION	VALUE
Date, Time	01/28/2017, 2:20pm; 25°C 50uL testing 02/04/2017, 2:30pm; 25°C, 60°C, 70°C, 75°C
Barometric Pressure	01/28/2017, 2:20pm; 763.270 mmHg 02/04/2017, 2:30pm; 765.556 mmHg
Room Temperature	01/28/2017, 2:20pm; 22.8°C (73°F) 02/04/2017, 2:30pm; 22.2°C (72°F)
Formula [29]	$C_{18}H_{32}O_2$
Molar Mass [29]	280.452 g/mol
Melting Point [29]	-6.9°C (19.58°F)
Flash Point [30]	113°C (235.4°F)
Boiling Point [29]	230°C (446°F)
Vapor Pressure [29]	8.68 x 10^{-7} mmHg at 25°C

4.5.2. Linoleic Acid Dispersion Plot

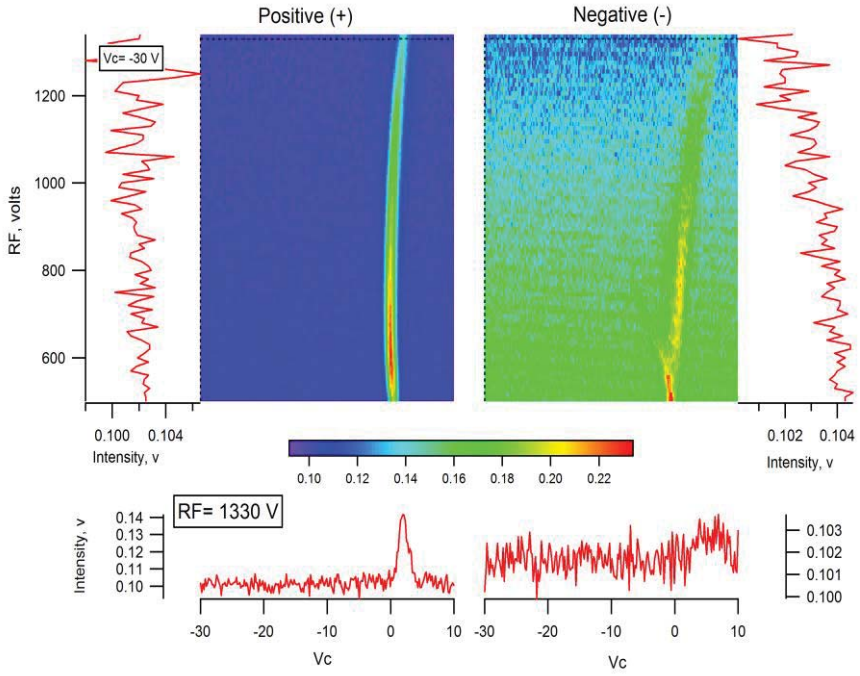

Figure 24 Linoleic Acid 25°C 50uL, Vrf Slider Set to 1330V

Linoleic acid samples were tested at 25°C, 60°C, 70°C and 75°C temperatures. The strongest response across the RF scan range was obtained at a sample temperature of 25°C for a 50uL volume and is shown in the dispersion plot of Figure 24. All Linoleic acid samples, except for the final sample at 25°C 50uL, were tested at 1uL volumes since previous testing at higher volumes saturated the system and required several days of clean air flowing through the system to remove trace amounts of the acid. Figures 25 and 26 show the Intensity versus Compensation Voltage response of Linoleic acid at an RF voltage of 1330V for all sample temperatures in the negative and positive ion modes, respectively. As mentioned previously, a RF voltage of 1330V was chosen for the 2-D graphs because it is the voltage that shows some peak separation between the other fatty acids.

For the negative ion mode, some differentiation from the baseline response was obtained for the samples at all the temperatures with the strongest response occurring for the 25°C 1uL

volumes, however, the SNR for all the negative ion samples is less than 3 and cannot be considered reliable indicators of detection. As a result, the negative ion mode fails to provide reliable detection for Linoleic acid at the temperatures and volumes tested.

For the positive ion mode, some differentiation from the baseline response was obtained for the samples at all the temperatures with the strongest response occurring for the 25°C 1uL volumes. However, except for the 25°C 50uL volume, the remaining temperature sample volumes have a SNR less than 3 and cannot be considered reliable indicators of detection. A very strong signal intensity response was obtained for the 25°C 50uL volume, as shown in Figure 27, having a SNR = 10.83. The 50uL major peak is located at a compensation voltages of 1.96V. Table 10 lists the compensation voltage and signal intensity for the response curve in Figure 27.

Table 10 Linoleic Acid Positive Ion Compensation Voltage at Peak Signal Intensity

TEMPERATURE	VOLUME	COMPENSATION VOLTAGE (Volts) Major Peaks	SIGNAL INTENSITY (Volts) Major Peaks	SNR Major Peaks
	Baseline (Average)		0.102000	
25°C	50uL	1.96	0.140044	10.83
Median		1.96	0.140044	10.83
Average (Tolerance)		1.96	0.140044	10.83

The measured response times of the 25°C 50uL sample are as follows:

- Sample introduction to initial detection = 5.38 seconds
- Sample introduction to peak intensity = 21.07 seconds

Upon removal of the sample, several days were required for the intensity level to decrease from its peak level and return to baseline levels due to the volume of acid injected into the DMS.

4.5.3. Linoleic Acid Sample Results at Vrf = 1330V

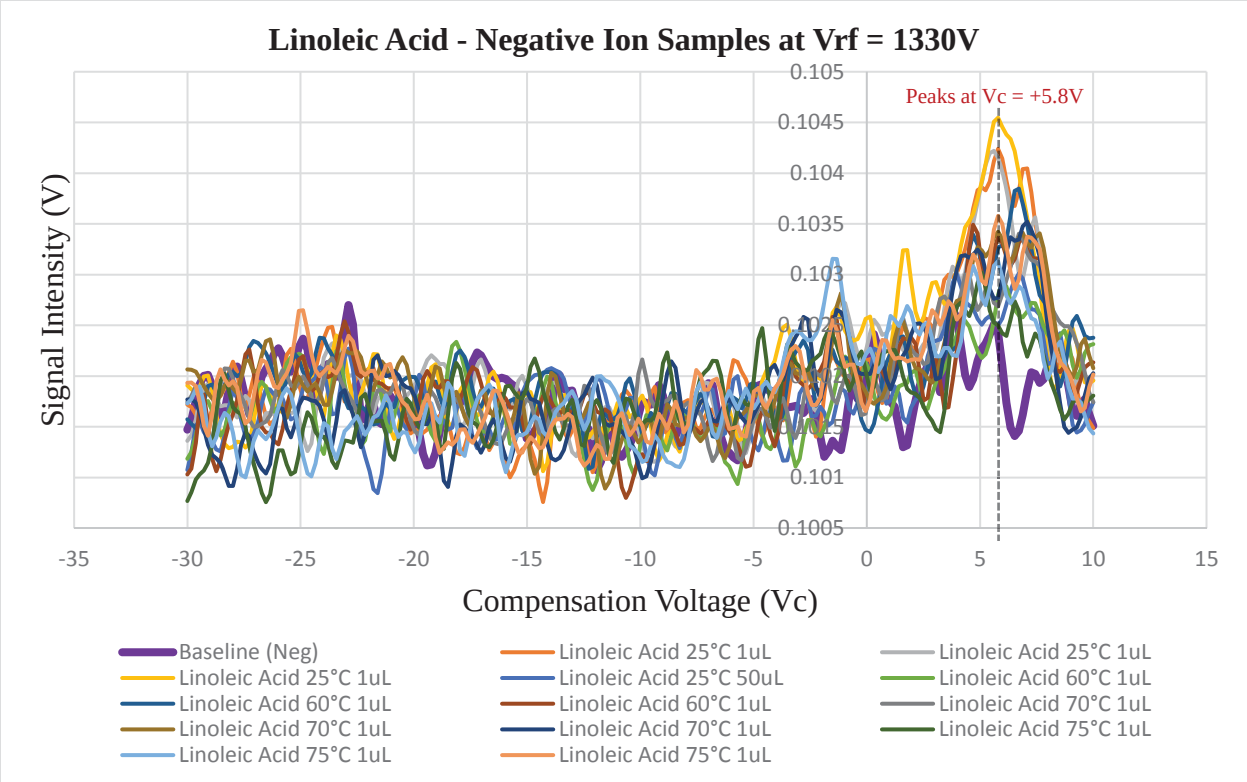

Figure 25 Linoleic Acid - Negative Ion Samples at Vrf = 1330V

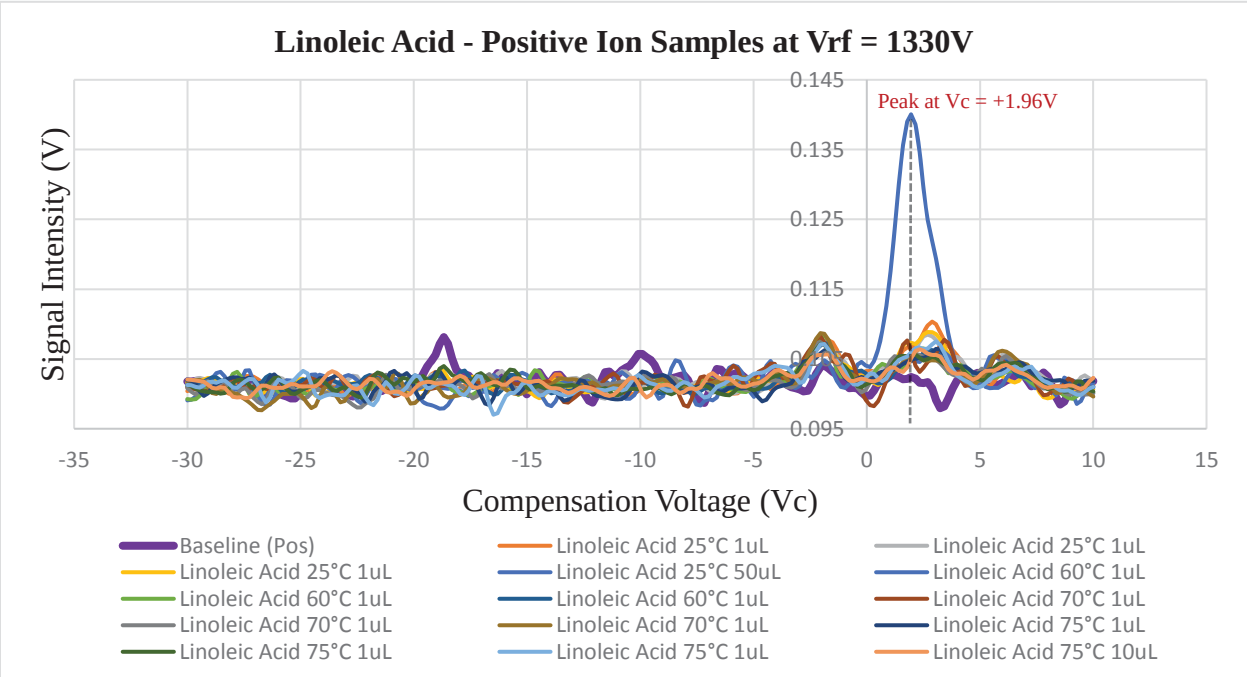

Figure 26 Linoleic Acid - Positive Ion Samples at Vrf = 1330V

4.5.4. Linoleic Acid Sample Results with Response at Vrf = 1330V

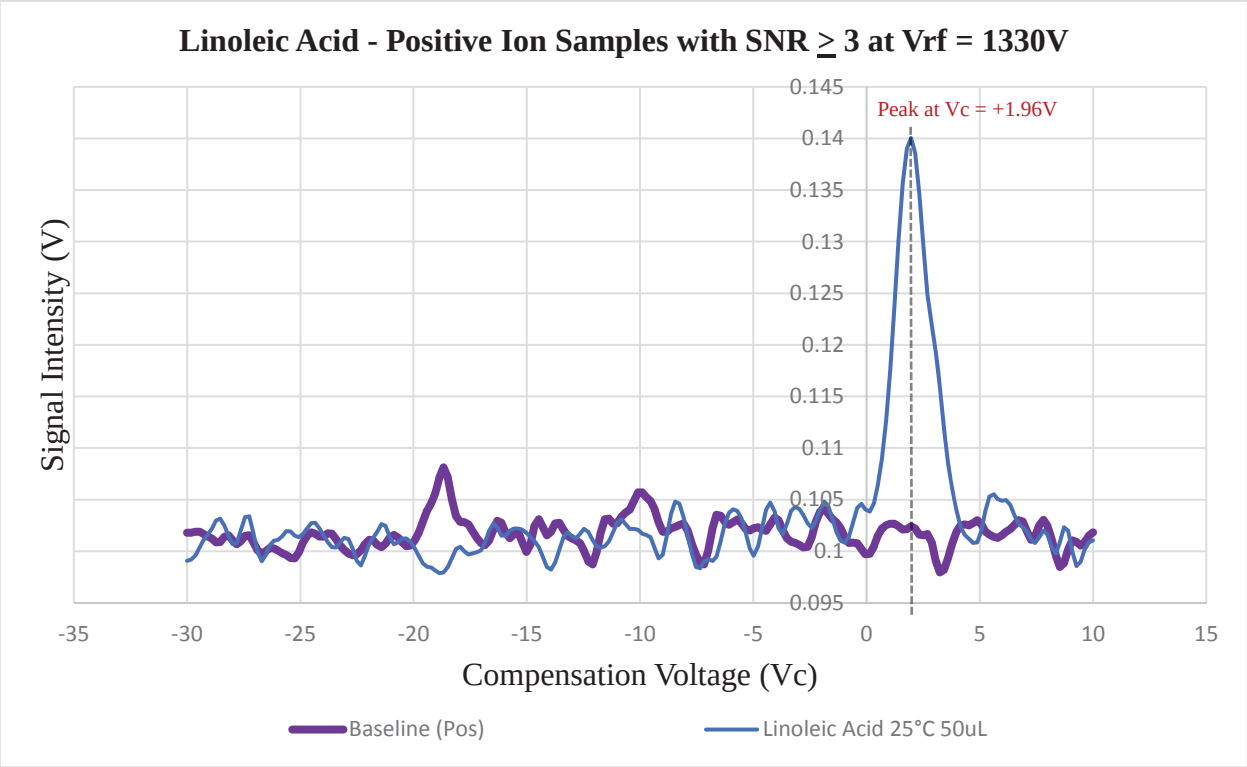

Figure 27 Linoleic Acid - Positive Ion Samples with SNR ≥ 3 at Vrf = 1330V

4.6. Fatty Acid Comparison Results at Vrf = 1330V

In the negative ion mode, only Stearic acid shows a response with a SNR ≥ 3 at a peak compensation voltage Vc = +4.7V at 75°C (Figure 18). For the samples and temperatures measured, Palmitic and Linoleic acids do not have sufficient response in the negative ion mode.

In the positive ion mode, the sample with the largest SNR from each fatty acid are combined into a single graph, as shown in Figure 28. Linoleic acid shows a unique peak compensation voltage Vc = +1.96V at 25°C. The peaks for Palmitic acid at 70°C and Stearic acid at 75°C are closer together with peak compensation voltages Vc = +5.98V and +6.53V, respectively. At Vc = +5.07V, Palmitic acid can be uniquely identified from Stearic acid since the Stearic acid response has declined to the DMS noise level.

Stearic acid cannot be uniquely identified at 75°C using only the positive ion mode of DMS. Figure 28 reveals that the response of Palmitic acid at 70°C is broad and crosses into the response region of Stearic acid, preventing the ability to distinguish between the two acids. The Palmitic acid data taken at 75°C, which is not included in the response graphs due to the data being suspect, indicates response into the Stearic acid range, confirming that Stearic acid response is not unique in the negative ion mode. However, Stearic acid uniquely responds in the positive ion mode, while Palmitic and Linoleic acids do not respond. Therefore, by using both the negative and positive ion modes of DMS for identification, Stearic acid can be uniquely identified from Palmitic and Linoleic acids.

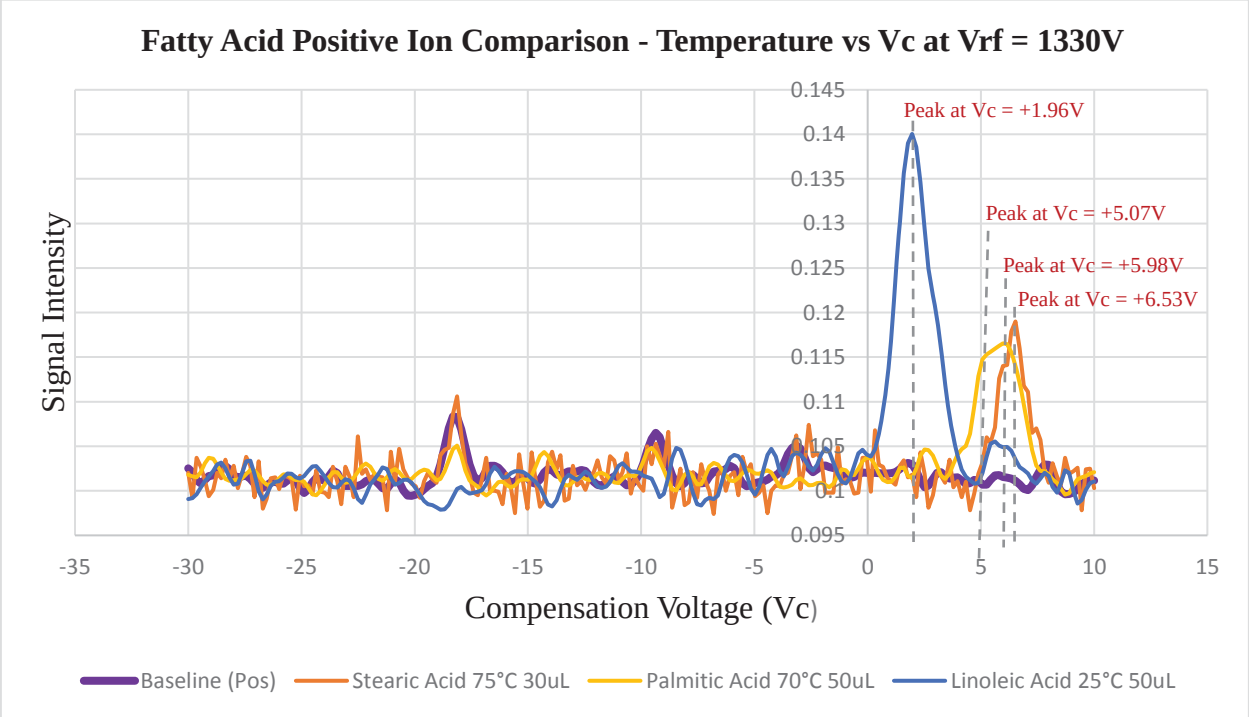

Figure 28 Fatty Acid Positive Ion Comparison - Temperature vs Vc at Vrf = 1330V

4.7. Limit of Detection for DMS Instrument

Equation 4 can be used to estimate the limit of detection for this DMS instrument using a known vapor pressure at a specified temperature. For the three fatty acids tested, the vapor pressures are published for a temperature of 25°C, however, only Linoleic acid responds near this temperature and will be used for the limit of detection calculation. The vapor pressure at the sample temperatures showing a signal response greater than 25°C are not readily published and, since vapor pressure changes non-linearly over temperature, it cannot be easily calculated at unpublished temperatures. However, the calculation using Linoleic acid will provide the reader with an approximate understanding on the order of magnitude for the DMS instrument sensitivity. A suggested improvement in determining the limit of detection with increased accuracy for the DMS instrument is discussed in Chapter 5: Discussion and Future Work.

In section 4.5.1. Linoleic Acid, the headspace concentration of Linoleic acid at 25°C is calculated to be 1.142 x 10^{-3} ppm. The SNR of the 25°C 50uL sample for Linoleic acid = 10.83. Choosing a SNR = 3 to be the minimum signal response required for reliable detection, Equation (6) can be used to estimate the limit of detection (LOD) for the DMS instrument using Linoleic acid.

$$\text{LOD} = \frac{\text{Linoleic Acid Gas Concentration}}{\text{SNR sample}} \text{ x SNR min} \tag{9}$$

$$\text{LOD} = \frac{1.142 \text{ x } 10^{-3} \text{ ppm}}{10.83} \text{ x } 3 = 0.316 \text{ x } 10^{-3} \text{ ppm} \tag{10}$$

$$\text{LOD} = 0.316 \text{ ppb}^{2}$$

[2] The method used to calculate the LOD for the DMS instrument is intended to provide the reader with an approximate sensitivity level within one to two orders of magnitude from the calculated result and should not be considered an absolute value. The published vapor pressure used in calculating Gas Concentration is specified at 25°C, however, the sample gas is introduced into a 50°C heated inlet tube, which will elevate gas temperature, thereby raising its vapor pressure, and can result in a less sensitive LOD value.

CHAPTER 5: DISCUSSION AND FUTURE WORK

5.1. Test Issues

Several issues were encountered during testing that may have affected the signal intensity response for the fatty acid samples. Each are described below.

Variations in the signal intensity response were observed for equivalent volumes of the same fatty acid, such as Palmitic acid. This is most likely due to the sampling method used. The glass syringe used for sampling was hand placed in the headspace just above the acid. Slight variations in this height may account for variations in the concentration sampled which can affect the signal intensity response.

The DMS used for this testing was designed for sensing gas samples with significantly higher vapor pressures, on the order of 10^{-3} mmHg or greater, which increases gas concentration and the probability of sample detection. The vapor pressures for the fatty acids tested are very low in comparison, which raises the difficulty in detecting the acid molecules and elevates the probability of persistent vapor collection on the flow path walls.

Due to the low volatility (vapor pressure) of the fatty acids, removal of the syringe containing the sample from the inlet port during testing required several minutes between samples to allow the signal intensity to return to near baseline levels. Several days of continuous filtered air flowing through the system was required between each fatty acid tested to ensure that trace amounts were removed from the system.

As mentioned in section 4.4.2. Palmitic Acid Dispersion Plot, the 75°C data taken on the last day of testing, 02/17/2017, is suspect due to observed intermittent behavior of the non-radioactive ion source. During the generation of the baseline dispersion plot, prior to introducing the Palmitic acid samples, a large gap in the baseline intensity response was observed in the positive ion mode, indicating that the ion source was not generating ions during that portion of the RF scan. A second baseline scan was generated for both ion polarities it appeared comparable to baseline scans run on previous days. However, during Palmitic acid 75°C sample testing, continued intermittent ion source behavior was observed and the data was discarded. Previously tested samples for Palmitic, Stearic and Linoleic acids is not suspect since no intermittent behavior of the ion source was observed prior to this test date. The ion source had inadvertently been left running after a system check several days prior and, as a result, operated continuously for approximately 72 hours. Under these conditions, the filaments used to generate the plasma in the ion source are significantly stressed and are most likely the cause of the observed intermittent behavior. Replacement of the ion source filaments requires disassembly of the instrument and was not available in a timely manner during the course of this work.

5.2. Conclusion

Stearic, Palmitic and Linoleic fatty acids can be uniquely identified using Differential Mobility Spectrometry by varying the sample temperature and ion mode polarity. Linoleic acid is uniquely identified at 25°C in the positive ion mode with a compensation voltage Vc = +1.96V. Palmitic acid can be uniquely identified at 70°C in the positive ion mode with a compensation voltage Vc = +5.07V. Stearic acid is uniquely identified at 75°C in the negative ion mode with a compensation voltage Vc = +4.7V. Approximate DMS detection times for the three fatty acids range from 2 to 6 seconds for initial detection up to 35 seconds for peak detection. The Limit of

Detection for the DMS instrument is estimated to be in the low ppb range based on the sampled concentration and SNR response of Linoleic acid.

5.3. Future Work

Suggested enhancements to the DMS instrument and sampling method to increase instrument sensitivity for fatty acid detection, improve response repeatability, and minimize cycle time between sample injections for chemicals with lower vapor pressure, includes the following: (1) Inserting a preheater in-line with the gas injection port to significantly raise the temperature of the introduced gas molecules (greater than the temperatures used in this work), will increase gas vapor pressure and potentially increase the probability of sample detection. (2) Using a controlled sample introduction method, such as a permeation tube, provides accurately controlled concentrations in the ppm to ppb range to be introduced into the DMS. Repeatability between samples is enhanced and a determination of the Limit of Detection for the DMS instrument can be resolved with increased accuracy. (3) Embedding integrated heaters within the sample path of the instrument and providing the ability to flow filtered air at a high rate throughout the system may allow for rapid removal of trace gasses.

Suggested investigation into the viability of using DMS for fatty acid biomarker detection includes: (1) Creation of compound mixtures of fatty acids and biomaterials, including those used in this work, which closely replicate the serum obtained from centrifuged human blood extractions, should be investigated and tested for fatty acid response differentiation. (2) The investigation and selection of a possible dopant gas that can combine with the target fatty acids which may enhance their differentiation response.

REFERENCES

[1] American Cancer Society, "How Common Is Breast Cancer?," 5 January 2017. [Online]. Available: https://www.cancer.org/cancer/breast-cancer/about/how-common-is-breast-cancer.html. [Accessed 5 March 2017].

[2] American Cancer Society, Inc., "For Women Facing a Breast Biopsy," September 2015. [Online]. Available: http://www.cancer.org/acs/groups/content/@editorial/documents/document/acspc-046345.pdf. [Accessed 18 September 2016].

[3] L. S. Eberlin, I. Norton, A. L. Dill, A. J. Golby, K. L. Ligon, S. Santagata, R. G. Cooks and N. Y. Agar, "Classifying Human Brain Tumors by Lipid Imaging with Mass Spectrometry," *American Association for Cancer Research,* vol. 72, no. 3, pp. 645-654, 2012.

[4] L. S. Eberlin, D. Orringer, I. F. Dunn, X. Liu, J. L. Ide, A. K. Jarmusch, K. L. Ligon, F. A. Jolesz, A. J. Golby, S. Santagata, N. Y. Agar and R. G. Cooks, "Ambient mass spectrometry for the intraoperative molecular diagnosis of human brain tumors," *Procedings of the National Academy of Sciences of the United States of America,* vol. 110, no. 5, pp. 1611-1616, 2013.

[5] N. Y. Agar, A. J. Golby, K. L. Ligon, I. Norton, V. Mohan, J. M. Wiseman, A. Tannenbaum and F. A. Jolesz, "Development of Stereotactic Mass Spectrometry for Brain Tumor Surgery," *Neurosurgery,* vol. 68, no. 2, pp. 280-290, 2011.

[6] University of Illinois at Urbana-Champaign, School of Chemical Sciences, "Mass Spectrometry Laboratory, Sample Submission," [Online]. Available: http://scs.illinois.edu/massSpec/submit/prep.php. [Accessed 4 March 2017].

[7] Sheffield Hallam University, "Gas Chromatography," [Online]. Available: http://teaching.shu.ac.uk/hwb/chemistry/tutorials/chrom/gaschrm.htm. [Accessed 4 March 2017].

[8] J. Balog, L. Sasi-Szabó, J. Kinross, M. R. Lewis, L. J. Muirhead, K. Veselkov, R. Mirnezami, B. Dezső, L. Damjanovich, A. Darzi, J. K. Nicholson and Z. Takáts, "Intraoperative Tissue Identification Using Rapid Evaporative Ionization Mass Spectrometry," *Science Translational Medicine,* vol. 5, no. 194, p. 194ra93, 2013.

[9] V. Tran, "IKnife," University of Rhode Island, Kingston, 2013.

[10] E. Nazarov, T. A. Postlethwaite and Q. Shi, "Planar Differential Mobility Spectrometry as a Powerful Tool for Gas Phase Ion Separation and Detection," Spectroscopy Solutions, [Online]. Available: http://www.spectroscopy-solutions.org/Information/Archive/Featured-Articles/2220-/Planar-Differential-Mobility-Spectrometry-as-a-Powerful-Tool-for-Gas-Phase-Ion-Separation-and-Detection. [Accessed 30 December 2016].

[11] Draper Laboratory, "Differential Mobility Spectrometry (DMS) - How do we build a rapid, portable, highly sensitive volatile chemical detection system?," [Online]. Available: http://www.draper.com/solution/differential-mobility-spectrometry-dms. [Accessed 11 September 2016].

[12] Chemring Sensors & Electronic Systems, "JUNO," [Online]. Available: http://www.chemringds.com/products/chemical-detection/juno.aspx. [Accessed 11 September 2016].

[13] S. Manolakos, F. Sinatra, L. Albers, K. Hufford, J. Alberti, E. Nazarov and T. Evans-Nguyen, "Differential Mobility Spectrometry for Inorganic Filtration in Nuclear Forensics," *Analytical Chemistry*, vol. 88, no. 23, pp. 11399-11405, 2016.

[14] United States Nuclear Regulatory Commission, "PART 31—GENERAL DOMESTIC LICENSES FOR BYPRODUCT MATERIAL," 1 October 2007. [Online]. Available: https://www.nrc.gov/reading-rm/doc-collections/cfr/part031/. [Accessed 3 March 2017].

[15] Draper Laboratory, "Stopping Killer Infections - Draper & Brigham and Women's Hospital Collaborate on Diagnostic Solution for Invasive Aspergillosis," [Online]. Available: http://www.draper.com/news/stopping-killer-infections. [Accessed 12 September 2016].

[16] W. Lv and T. Yang, "Identification of possible biomarkers for breast cancer from free fatty acid profiles determined by GC–MS and multivariate statistical analysis," *Clinical Biochemistry*, vol. 45, no. 1-2, pp. 127-133, 2011.

[17] V. Pala, V. Krogh, P. Muti, V. Chajès, E. Riboli, A. Micheli, M. Saadatian, S. Sieri and F. Berrino, "Erythrocyte Membrane Fatty Acids and Subsequent Breast Cancer: a Prospective Italian Study," *Journal of the National Cancer Institute*, vol. 93, no. 14, pp. 1088-1095, 2001.

[18] M. SaadatianElahi, T. Norat, J. Goudable and E. Riboli, "Biomarkers of dietary fatty acid intake and the risk of breast cancer: A metaanalysis," *International Journal of Cancer*, vol. 111, no. 4, pp. 584-591, 2004.

[19] Wikipedia, "Gas chromatography," 11 November 2016. [Online]. Available: https://en.wikipedia.org/wiki/Gas_chromatography. [Accessed 22 November 2016].

[20] A. A. Shvartsburg, Differential Ion Mobility Spectrometry: Nonlinear Ion Transport and Fundamentals of FAIMS, Boca Raton: CRC Press, 2008.

[21] E. G. Nazarov, "Differential Ion Mobility Mass spectrometry – The next 5 years - Status and history of development," in *Ion Mobility Mass Spectrometry - The Next Five Years*, Norwalk, CT: Owlstone, Inc, 2016, pp. 10-16.

[22] B. B. Schneider, E. G. Nazarov, F. Londry, P. Vouros and T. R. Covey, "DIFFERENTIAL MOBILITY SPECTROMETRY/MASS SPECTROMETRY HISTORY, THEORY, DESIGN OPTIMIZATION, SIMULATIONS, AND APPLICATIONS," *Mass Spectrometry Reviews*, pp. 1-51, 2015.

[23] E. Krylov, "Comparison of the planar and coaxial field asymmetrical waveform ion mobility spectrometer (FAIMS)," *International Journal of Mass Spectrometry*, no. 225, pp. 39-51, 2003.

[24] Johns Hopkins Bloomberg School of Public Health, "Lecture 5: Gases and Vapors," 2006. [Online]. Available: http://ocw.jhsph.edu/courses/PrinciplesIndustrialHygiene/PDFs/Lecture5.pdf. [Accessed 27 February 2017].

[25] National Center for Biotechnology Information, "PubChem Compound Database; CID=4133," [Online]. Available: https://pubchem.ncbi.nlm.nih.gov/compound/4133 . [Accessed 17 February 2017].

[26] National Center for Biotechnology Information, "PubChem Compound Database; CID=5281," [Online]. Available: https://pubchem.ncbi.nlm.nih.gov/compound/5281 . [Accessed 18 February 2017].

[27] National Center for Biotechnology Information, "PubChem Compound Database; CID=985," [Online]. Available: https://pubchem.ncbi.nlm.nih.gov/compound/985. [Accessed 19 February 2017].

[28] Sigma-Aldrich, "P0500 Safety Data Sheet," [Online]. Available: http://www.sigmaaldrich.com/catalog/product/sigma/p0500?lang=en&region=US. [Accessed 19 February 2017].

[29] National Center for Biotechnology Information, "PubChem Compound Database; CID=5280450," [Online]. Available: https://pubchem.ncbi.nlm.nih.gov/compound/5280450 . [Accessed 20 February 2017].

[30] Sigma-Aldrich, "L1376 Safety Data Sheet," [Online]. Available: http://www.sigmaaldrich.com/catalog/product/sigma/l1376?lang=en&region=US. [Accessed 20 February 2017].

APPENDIX A: GLOSSARY

DC	Direct Current
Headspace	The space just above the liquid or solid in a closed vial or container
Hz	Hertz
MHz	Megahertz
mmHg	Pressure measurement in Millimeter of Mercury
mV	Millivolt = 1×10^{-3} Volts
NA	Not Applicable
NIST	National Institute of Standards and Technology
PN	Part Number
PSI	Pounds per Square Inch
PTFE	Polytetrafluoroethylene
RF	Radio Frequency
sccm	Standard Cubic Centimeters per Minute
USPTO	United States Patent Trade Office
uV	Microvolt = 1×10^{-6} Volts